Simulation of Ca^{2+} transients in the continuum of mammalian skeletal muscle fiber types

Oscar Andrés Rincón Cardeño

Director

Prof. Marco Antonio Giraldo. PhD

Biophysics Group, Institute of Physics, University of Antioquia

Co-director

Prof. Juan Camilo Calderón. PhD

Physiology and Biochemistry Research Group-PHYSIS, Faculty of Medicine, University of Antioquia

Institute of Physics

Faculty of Exact and Natural Sciences

University of Antioquia

2021

To my parents Liliam and David

Acknowledgment

I would like to thank the professors Juan Camilo Calderón and Marco Antonio Giraldo for allowing me to be part of the Biophysics Group and the Physiology and Biochemistry Research Group during this work. To Andrés Felipe Milan Tabares, since the results of his master thesis "*In situ calibration of the Mag-Fluo-4 fluorescent indicator in mouse muscle cell*" permitted me to include novel experimental data in this work. Also, to my classmates from the master program in physics for their company during the writing of this work. This work was funded by CODI-University of Antioquia 2015-7858.

Abstract

Mathematical models have allowed a better understanding of the excitation-contraction coupling (ECC) during the activation of skeletal muscle fibers. Experiments with isolated mammalian muscle fibers loaded with Mag-Fluo-4 have revealed differences in the kinetics of the Ca^{2+} transients, as key experimental manifestation of the ECC, in the continuum of fiber types. However, a comprehensive mathematical description of the ECC, that considers most of the Ca^{2+}-binding sites (e.g. parvalbumin, troponin, the dye, transporters, and pumps) in that continuum of fiber types has not been developed. Also, besides the classical mechanisms, namely parvalbumin (PV) and sarcoplasmic reticulum Ca^{2+} ATPase (SERCA), it has been determined that the Ca^{2+} removal from cytoplasmic compartment also depends on the mitochondrial Ca^{2+} movements and the Na^{+}/Ca^{2+} exchanger (NCX) when the Ca^{2+} concentration is high in the cytoplasm and the PV and SERCA are saturated.

In this work, changes in the concentration of Ca^{2+} through the sarcomere due to the ion's movement were simulated for different mammalian fiber types (I, IIA, IIX/D and IIB) using single Ca^{2+} transients experimentally measured in mouse fibers loaded with the fast fluorescent indicator Mag-Fluo-4 AM at room temperature. Considering an estimated dye concentration of 246.5 μM, we found that the amplitude of the peak of the release rate of Ca^{2+} from the sarcoplasmic reticulum of the fibers type IIA, IIX and IIB, was 22.7%,

437.6% and 528.5%, respectively, higher than the type I. The cytoplasmic peak Ca^{2+} concentration was 14.32 µM, 14.32 µM, 10.96 µM and 8.63 µM. On the other hand, the mitochondrial peak Ca^{2+} concentration was 10.3%, 77.8% and 79.6% lower in the fibers type IIA, IIX and IIB than in the type I. The Ca^{2+} extruded from the cytoplasm by the NCX was 27.1%, 466.1% and 405.1% higher in fibers type I, IIX and IIB than in the type IIA. The decay phase of the Ca^{2+} transient can be fitted with a biexponential function (with τ_1 and τ_2). An increase of 50% in the parvalbumin content differentially changed the τ_1 of the IIB-IIX group by -6.0% and of the IIA-I group by 16.2%, whilst the τ_2 always decreased, by 26.1% in the IIB-IIX group and 6.1% in the IIA-I group.

In conclusion, we presented for the first time a comprehensive model of Ca^{2+} movements based on kinetic parameters of the four mammalian fiber types and the molecular machinery involved in the ECC, including the mitochondria and the NCX. The proposed model allowed us to gain insight into the kinetics of the Ca^{2+} transients obtained with a fast Ca^{2+} dye, for the continuum of muscle fiber types.

Keywords:

Skeletal muscle, fiber types, Ca^{2+} transients, mitochondria, Na^{+}/Ca^{2+} exchanger, mathematical simulation.

Content

List of figures

List of tables

Abbreviations

AP Action potential

ATP Adenosine triphosphate

B Mitochondrial buffer

Ca^{2+} Calcium ions

CQS Calsequestrin

D Diffusion coefficient

DHPR Dihydropyridine receptor

ECC Excitation contraction coupling

F Fluorescence intensity

$\boldsymbol{F_{rest}}$ Resting fluorescence intensity due to $[Ca^{2+}]$ in the cytosol

$\boldsymbol{F_{min}}$ Minimum fluorescence intensity that an intracellular fluorescent dye can reach into the cell

$\boldsymbol{F_{min}}$ Maximum fluorescence intensity that an intracellular fluorescent dye can reach into the cell

FDB *Flexor digitorum brevis*

FDHM Full duration at half-maximum

K_d Dissociation constant

Mg^{2+} Mg^{2+} ions

MCU Mitochondrial Ca^{2+} uniporter

MT-I Morphology type I of Ca^{2+} transient in skeletal muscle fibers

MT-II Morphology type II of Ca^{2+} transient in skeletal muscle fibers

NCX Na^{2+}/Ca^{2+} exchanger

NRMSE Normalized root mean square error

ODE Ordinary differential equation

PV Parvalbumin

Trop Troponin

T-tubule Transverse tubule

SERCA Sarcoplasmic reticulum Ca^{2+} ATPase

SR Sarcoplasmic reticulum

RyR Ryanodine receptor

V_{max} Maximum rate of enzymatic chemical reaction

ΔF Change of fluorescence intensity above the resting fluorescence

[] Quantity between brackets represent concentration

Chapter 1

Introduction

In the skeletal muscle fiber, the action potentials (AP) leads to contractions mediated by the release of Ca^{2+} ions from the sarcoplasmic reticulum (SR) (Ridgway & Ashley, 1967). Experiments on electrically elicited Ca^{2+} transients measured in mammalian muscle fibers loaded with fluorescent indicators have revealed differences in the kinetic parameters associated with the type of fiber and the molecular machinery involved in the Ca^{2+} transients (Calderón et al., 2010).

The excitation contraction coupling (ECC) phenomenon represents the relation between the electrical events occurring in the plasma membrane and the Ca^{2+} release from the SR, which leads to the muscle contraction (Fig. 1). The sequence of events in skeletal muscle fibers involves: (1) initiation and propagation of an AP along the plasma membrane, (2) radial spread of the potential along the transverse tubule (T-tubule) system, (3) detection of changes in the membrane potential mediated by the dihydropyridine receptors (DHPR, L-type Ca^{2+} channel CaV1.1), (4) allosteric interaction of the DHPR with the SR ryanodine receptors (RyR), (5) release of Ca^{2+} from the SR and transient increase of Ca^{2+} concentration in the myoplasm (cytoplasm in muscle cells), (6) transient activation of the myoplasm Ca^{2+} buffering system, formed by proteins such as the troponin (Trop), parvalbumin (PV) and the Ca^{2+}-binding molecules such as the adenosine triphosphate (ATP), and the contractile apparatus, followed by (7) disappearance of Ca^{2+} from the

myoplasm mediated by its movement to the mitochondria (MITO), its transport outside the cell by the Na^{+}/Ca^{2+} exchanger (NCX) and its final reuptake by the SR through the SR Ca^{2+} adenosine triphosphatase (SERCA) (Calderón et al., 2014a). Store-operated Ca^{2+} entry (SOCE) allows Ca^{2+} enter the fiber, as a response to the intra SR Ca^{2+} sensing function of the stromal interaction molecules (STIM) (Stiber et al., 2008). In fast twitch fibers, SOCE acts in a transient fast mode during an individual AP and after each AP in a train of stimulations (Koenig et al., 2018).

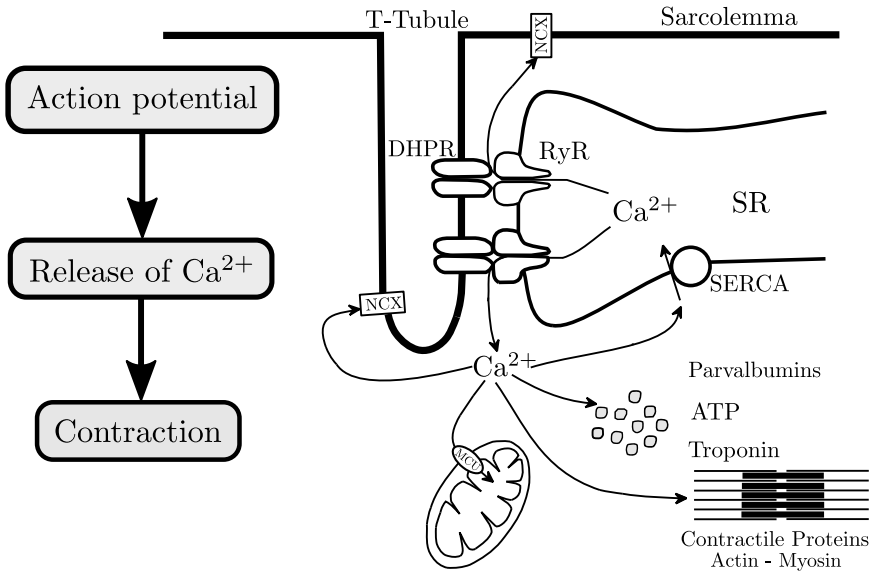

Fig. 1. Illustration of the Ca^{2+} release and removal mechanisms. Taken and modified from the supplementary material of Calderón et al. (2014).

Detailed works have permitted the identification of a continuum of fiber types, divided into two groups, fast and slow. The slow twitch fibers have important differences in the ECC when compared to the fast twitch fibers. Two main differences are the quantity and kinetics of the proteins present in the cytoplasm (Calderón et al., 2014a). In terms of quantity, one of the most

notable differences is the concentration of parvalbumin (PV), being almost negligible in slow-twitch fibers and up to 0.43 mM in the fastest (Heizmann, 1984). It is known that these high concentrations of PV are involved in the muscle relaxation process (Calderón et al., 2014a; Heizmann et al., 1982). Higher amount of SERCA in the fast fibers have also been known for three decades already (Ferguson & Franzini-Armstrong, 1988; Leberer & Pette, 1986).

Mathematical models that integrate information obtained on mammalian ECC under different experimental conditions have been used to simulate Ca^{2+} transients in slow-twitch and fast-twitch fibers (Stephen M. Baylor & Hollingworth, 2007b; Stephen Hollingworth et al., 2012). A better understanding of the kinetics of Ca^{2+} and its relationship with the amount of proteins in the cytoplasm has thus been allowed. A more complete model that compares the kinetics of slow and fast-twitch fibers was presented by Baylor and Hollingworth (Stephen M Baylor & Hollingworth, 2012). The model, however, was built on data of fibers whose nature (fast or slow) was not certain, since the authors did not use gold-standard techniques, like i.e., myosin heavy chain detection, to classify the fibers. Furthermore, it did not include the role of MITO and NCX in the ECC, basically because they were largely ignored by that time. The dependency of Ca^{2+} removal from the cytosolic compartment on the kinetics of PV and SERCA kinetics and content of mammalian fibers of slow-twitch and fast-twitch have been previously described in a mathematical model (Stephen M Baylor & Hollingworth, 2012). However, this removal from the cytoplasmic compartment also depends on the MITO and the NCX. Since the NCX has low-affinity and high transport capacity compared to the SERCA, it is a more appropriate mechanism for Ca^{2+} removal at higher [Ca^{2+}] (Balnave & Allen, 1998). Also, the influence of the MITO to the regulation of Ca^{2+} in the cytosol may be

relevant in slow-twitch fibers, given their higher content in slow fibers. A major drawback of the mentioned papers is that they used an oversimplified dichotomic approach (slow of fast), to model the ECC, even when there are at least four fiber types, I, IIA, IIX/D and IIB.

The mitochondrial effective volume is a morphological difference between fiber types, being higher in the slow twitch fiber (Jackman & Willis, 1996; Schwerzmann et al., 1989). Partly because of this, slow-twitch fibers are more resistant to fatigue (Schwerzmann et al., 1989). This is evidenced by an alteration of the kinetics of the decay phase of the Ca^{2+} transients when mitochondrial Ca^{2+} uptake is inhibited (Calderón et al., 2014b; Stephen Hollingworth et al., 2012).

We rely on the model initially proposed by Cannell and Allen (1984) and on models that use a similar structure to describe the movement of Ca^{2+} and compare the kinetics of slow-twitch and fast-twitch fibers (Stephen M Baylor & Hollingworth, 2012). In this type of models, the sarcomere is assumed to be cylindrical and divided into compartments with radial symmetry. Thus, the change in the concentration of Ca^{2+} of each compartment generated by a twitch or by a series of stimuli, is 3-D considered.

Overcoming some of the above mentioned limitations, a recent model of skeletal muscle ECC interestingly included the MITO and proteins such as the mitochondrial Ca^{2+} uniporter (MCU) and the mitochondrial NCX (NCE) (Marcucci et al., 2018). In fact, the model of Marcucci et al. (2018) included a description of $[Ca^{2+}]$ changes in the cytosolic compartment, SR and MITO. A validation of this model is obtained by the determination of $[Ca^{2+}]$ in the compartments by ratiometric, slow probes. In the case of the cytosolic compartment, $[Ca^{2+}]$ was measured with Fura-2. However, the Fura-2 dye

seem not to reliably track the kinetics of fast, large and brief Ca^{2+} transients such as those found in skeletal muscles. The most suitable dyes to study ECC in skeletal muscle seem to be the low affinity, fast Ca^{2+} dyes, like Mag-Fura-2 and Mag-Fluo-4 (Stephen M. Baylor & Hollingworth, 2011; Calderón et al., 2014a). Also, the amplitude achieved by a single Ca^{2+} transient of about 0.4 µM is very low compared to previous reported values of about 3.9 µM in measurements with the dye fluo-3 AM in intact single muscle fibers of the tropical toad Leptodactylus insularis (Caputo & Bolaños, 1994), 4.6 µM with the dye Mag-Fura-2 in cut fibers of rat extensor digitorum longus muscle (EDL) (Delbono & Stefani, 1993), and 16 µM with the dye Mag-Fura-2 in fast-twitch muscle fibers (Stephen Hollingworth et al., 2012). Also, the lack of a fiber type approach limits the extent of impact of the Mariucci's work.

In this work we use measurements with the fluorescent indicator Mag-Fluo-4 AM and a multi compartment model to estimate the Ca^{2+} movements produced during single and tetanic Ca^{2+} transients in four mammalian skeletal muscle fiber types. This allows us to make a simulated comparison of the Ca^{2+} movement between different fiber types, including the variations in the mitochondrial $[Ca^{2+}]$, the sarcolemmal NCX, and their influence on the cytoplasmic Ca^{2+} regulation.

.

Chapter 2

Preliminaries

In this chapter we briefly introduce the skeletal muscle physiology and the classification of fiber types. We later presented measurements of the [Ca^{2+}] changes in skeletal muscle fibers with fluorescent indicators and the resulted insights that motivated our simulations. Then we described the models that have been used to describe the mechanisms involved in ECC and the models used to convert fluorescent measurements into [Ca^{2+}].

2.1 Skeletal muscle

Mammalian muscles are divided into three main categories: smooth, cardiac and skeletal. Skeletal and cardiac muscle are also called striated muscles, since when they are observed under a microscope it is possible to observe stripes that are transverse to the longer axis. Skeletal muscles are composed by a set of muscle cells, also called fibers. These fibers have an almost cylindrical shape and belong to a group of cells that are electrically excitable, with contractile capacity responsible for the main part of voluntary motion in mammals. Altogether, it accounts for about 40% of body weight (Rolfe & Brown, 1997).

Skeletal muscles fibers can be distinguished on the basis of their color as red or white and their contractile properties as fast and slow since the first half of the 19th century (Needham, 1926; Ranvier & M L., 1873). The slow and fast fibers can also be named as type I and type II fibers, respectively (Dubowitz

& Pearse, 1960; Engel, 1998). This initial classification has become more complex since the development of new methods to differentiate fibers types in the last decades.

Four fiber types have been distinguished based on the presence measurements of the myosin heavy chain (MHC) isoform: I, IIA, IIX/D and IIB (Calderón et al., 2010; Schiaffino et al., 1989). A resulting question from this classification is: how do the proteins involved in the ECC mechanism and Ca^{2+} transient kinetics change according to the fiber types? insight have emerged from measurements using fluorescent Ca^{2+} indicators.

2.2 Measurements of Ca^{2+} transients during ECC with fluorescent indicators in skeletal muscle fibers

The Ca^{2+} plays an important role in biological systems. For the ECC, Ca^{2+} serves as a messenger that couples the electrical excitation at the skeletal muscle fiber membrane to the contractile machinery inside the fiber. In general, when cytoplasmic $[Ca^{2+}]$ rises, the muscle contracts, and when $[Ca^{2+}]$ decreases, the muscles relaxes (Berchtold et al., 2000).

The rise and fall of free Ca^{2+} produced in the cytoplasm during the activation of the fibers, so called Ca^{2+} transient, can be experimentally measured by using a Ca^{2+} sensitive fluorescent indicator such as Mag-Fura-2 or Mag-Fluo-4 AM (Stephen M. Baylor & Hollingworth, 2011). The light intensity signals as a function of time are recorded and used to estimate the changes in $[Ca^{2+}]$.

Fluorescent indicators can be divided according to whether they are ratiometric or non-ratiometric. Non-ratiometric dyes, such as Mag-Fluo-4, can be excited with visible light and are characterized because when they bind to Ca^{2+} the wavelength at which they present the maximum excitation or emission does not change. Ratiometric indicators, on the other hand, show

not only a change in intensity, but also in the wavelength at which the maximum excitation or emission occurs.

To reliably estimate the amplitude and the time course of the change in [Ca^{2+}], an indicator of fast response and low affinity for Ca^{2+} is required (Hirota et al., 1989; Konishi et al., 1993). An indicator of Ca^{2+} can be considered of low affinity when it has a dissociation constant (Kd) for Ca^{2+}>25 μM (Stephen M. Baylor & Hollingworth, 2011). Dyes such as Mag-Fura-2 and Mag-Fluo-4 have low affinities for Ca^{2+}, however, Mag-Fura-2 is technically more difficult to use and has lower quantum efficiency when Ca^{2+} binds compared to Mag-Fluo-4 (Calderón et al., 2014a).

The basic unit of mechanical activity is the twitch, in which a single AP on the surface membrane of the fiber elicits a brief contractile response. Intracellular Ca^{2+} transients can thus be experimentally elicited by applying supra-threshold rectangular current pulses (0.6–1.4 ms) through two silver or platinum plate electrodes placed on either side along the experimental chamber (Fig. 2).

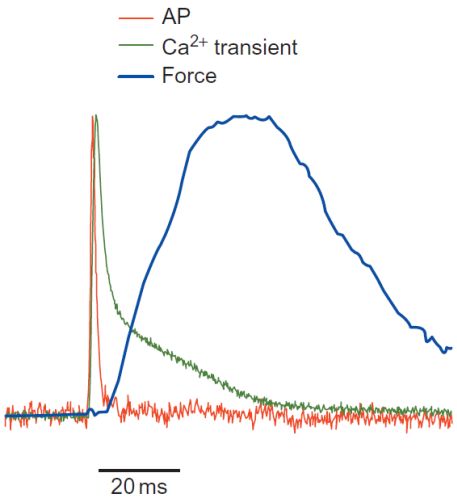

Fig. 2. Simultaneous measurements of action potential (AP), Ca^{2+} transient and force in fibers of the *flexor digitorum muscle* (FDB) of mouse. Note that the electrical phenomenon precedes the Ca^{2+} appearance in the cytosol, which in turn starts a couple of milliseconds before the initial rise in tension. The amplitude of the three signals was normalized for the sake of simplicity. Taken from Hill and Olon (2012).

The Ca^{2+} transient kinetics is produced by several mechanisms involving a great number of proteins that determine the different characteristics such as rise time, peak amplitude, half-width and time course of decay. Thus, the release and reuptake mechanisms of Ca^{2+} have different roles depending on the fiber type (Calderón et al., 2010, 2014b), which means that there are biochemical and structural differences according to the fiber types, such as the cytosolic Ca^{2+} buffers concentration and reaction rates between Ca^{2+} and the binding proteins that play a role during the ECC phenomenon.

The molecular machinery involved in the ECC includes ion channels, transporters, and pumps. Specifically, the higher content of the DHPR and RyR in fast fibers explains the differences in the rising phase of the Ca^{2+} transients, since they produce the activation of the Ca^{2+} channels associated to the Ca^{2+} release. Whereas the higher content of the PV transporter and the higher content and kinetics of SERCA pump explains the lower decay time required for fast fibers during a Ca^{2+} transient (Calderón et al., 2010). Other proteins such as mitochondria and NCX also have an influence in the decay rate, however with a minor role (Calderón et al., 2014b). Fig. 3 shows experimental measurements of the fluorescence intensity (*F*) in different fiber types (I, IIA, IIX/D and IIB) produced by an AP when measured with Mag-Fluo-4.

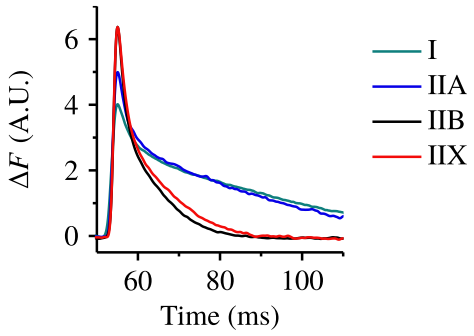

Fig. 3. Fluorescence intensity obtained during single Ca^{2+} transient's measurements in different fiber types (I, IIA, IIX/D and IIB) of mouse. Redrawn from Calderón et al. (2014).

The Ca^{2+} transient measurements can be classified into two different morphologies according to their kinetics (Calderón et al., 2009, 2010, 2014a). Morphology type I (MT-I), characteristic of fibers type I and IIA, has a lower peak, is broader and slower during the decay phase compared to morphology type II (MT-II). On the other hand, MT-II, defines fibers type IIX and IIB (Fig 2. B).

The Ca^{2+} transients produced by a repetitive stimulation, so called tetanic Ca^{2+} transients, also have a typical appearance. Tetanic Ca^{2+} transients of fibers types I and IIA show a staircase morphology (MT-I), whilst fibers type IIX and IIB are characterized by a first large peak followed by a plateau (MT-II). Fig. 4. shows the fluorescence intensity obtained during (A) single Ca^{2+} transients measurements of different fiber types (I, IIA, IIX/D and IIB) and tetanic Ca^{2+} transients in fiber types I (MT-I, B) and morphology type IIB (MT-II, C) for both morphologies during a train of APs with a frequency of 100 Hz and variable duration, from a single twitch to tetanic stimulus with a duration of 350 ms.

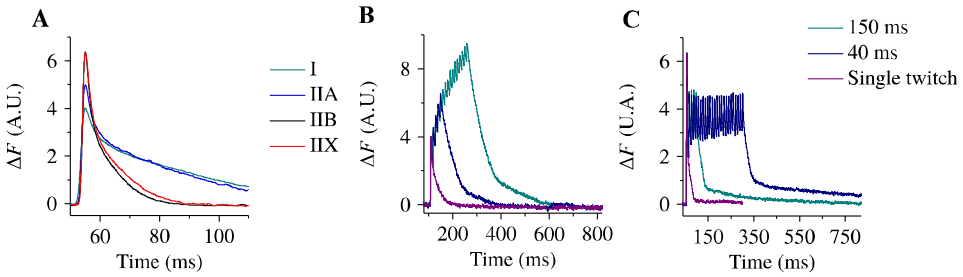

Fig. 4. Fluorescence intensity obtained during (A) single Ca^{2+} transients measurements of different fiber types (I, IIA, IIX/D and IIB) and tetanic Ca^{2+} transients in fiber types I **(**MT-I, B) and morphology type IIB **(**MT-II, C). Redrawn from Calderón et al. (2014).

In fibers MT-I, the decay of the last Ca^{2+} transient peak can be fitted by a single exponential function of the form: $F = C + A_1 \cdot [-e^{-t/\tau_1}]$. On the other hand, fibers with MT-II have tetanic Ca^{2+} transients whose decay can be fitted with high proximity with a bi-exponential function $F = C + A_1 \cdot [-e^{-t/\tau_1}] + A_2 \cdot [-e^{-t/\tau_2}]$ (Calderón et al., 2009, 2010). Where A_1 and A_2 represent the amplitudes. Thus, the decay phase of MT-I transients can be quantified by the time constant τ_1, while with τ_1 and τ_2 for MT-II transients Fig. 5.

The different fiber types also show different resistance to fatigue. The amplitude of the whole tetanic Ca^{2+} transient, when so called slow dyes are used, differentially changes in slow and fast fiber types. This behavior is presumably associated to the inactivation of the Ca^{2+} release mechanism (when the cytoplasmic concentration of Ca^{2+} is higher). Furthermore, since in fast fibers the SERCA and PV concentration is higher, a grater fatigue effect is expected.

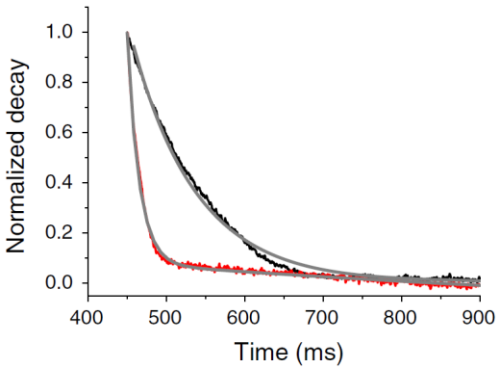

Fig. 5. Normalized decay phase of tetanic Ca^{2+} transients in fiber types I **(**MT-I, black line) and type IIB **(**MT-II, red line) fitted by a single and double exponential function (gray line), respectively. Taken from Calderón et al. (2014).

The Ca^{2+} measurements with fluorescent indicators have been an important method to study the sequence of events that occur during the ECC, however, there are questions that still remain unanswered, such as: i) what is the difference in the release of Ca^{2+} and peak [Ca^{2+}] among all four different fiber types? ii) what is the influence of the NCX and mitochondria in the Ca^{2+} removal from the cytoplasm? iii) what is the kinetics of Ca^{2+} movements in different compartments of the four fiber types?

2.3 Modelling of Ca^{2+} movements during ECC in skeletal muscle fibers

Mathematical models have been used to describe the Ca^{2+} kinetics in skeletal muscle fibers. Binding and enzymatic reactions, in combination with diffusion, are the basic building blocks to model the intracellular Ca^{2+} dynamics. For example, the reaction-diffusion equation in cylindrical coordinates and the *law of mass action* have been used to describe the diffusion of Ca^{2+} in the cytoplasm and its reaction with the binding sites in skeletal muscle. The Michaelis-Menten kinetics have allowed a description of the SERCA and the MCU in models of Ca^{2+} movements (S M Baylor &

Hollingworth, 1998; Cannell & Allen, 1984; Hollý & Poledna, 1989; Marcucci et al., 2018). Also, mathematical expressions to convert the measurements of fluorescent intensity into [Ca^{2+}] have been obtained from the comprehension of the reaction between Ca^{2+} and the fluorescent indicator with the *law of mass action*. A description of these mathematical models, which were used in the computational simulations in this thesis are included in the next sub-sections.

2.3.1 Reaction diffusion equation

Consider a chemical species C whose concentration *c* varies in both time and space in a region Ω with a volume *V*. The conservation of C can be expressed in words as (Fall, 2004; James & Keener, 2009):

rate of change of C = rate of production of C + accumulation of C due to transport.

The total amount of C at any time *t* in a region of space Ω can be obtained by integrating *c* over the volume *V*:

$$\text{rate of change of C} = \frac{d}{dt}\int_{\Omega} c\, dV\,, \tag{1}$$

assuming that C is free to move about randomly, so that C moves in and out of the volume by passing through the volume's surface S. If *J* is the flux density of C and **n** is the outward unit normal to the boundary of Ω we get that:

$$\text{accumulation of C due to transport of C} = -\frac{d}{dt}\int_{\Omega} J\cdot\mathbf{n}\, dA\,,$$

where *dA* is the surface integration element. Because **n** is the outward normal, $J \cdot \mathbf{n}$ is positive when the motion is from inside to outside, which accounts for the negative sign in this equation. According to the divergence theorem:

$$\text{accumulation of C due to transport of C} = -\frac{d}{dt}\int_{\Omega} \nabla \cdot \mathrm{J}\, dV \ . \qquad (2)$$

Considering *f* as the local production density of C per volume unit:

$$\text{rate of production of C} = \frac{d}{dt}\int_{\Omega} f\, dV \ . \qquad (3)$$

From Eqs. 1, 2 and 3 we obtain the following expression:

$$\frac{dc}{dt} = f - \nabla \cdot J \qquad (4)$$

Many physiological mechanisms depend on diffusion. If a molecule is not constrained, it will move randomly in three dimensions. However, for a gradient of *c*, it is reasonably intuitive that the chemical species will move from regions of high concentration to regions of low concentration. Thus:

$$\frac{dc}{dt} = J = -D\nabla c \ , \qquad (5)$$

where the rate of change of *c* over the time is a flux *J* and the proportionality constant *D* is called diffusion coefficient of the C molecules. The negative sign indicates the direction of the flux, from regions of high concentrations to regions of low concentration. Eq. 5, for chemical species, is called *first Fick's law*, and when it is applied Eq. 4 becomes the reaction diffusion equation:

$$\frac{dc}{dt} = \nabla \cdot (D\nabla c) + f$$

or, if *D* is a constant,

$$\frac{dc}{dt} = D\nabla^2 c + f. \tag{6}$$

The reaction diffusion equation describes the concentration variations of one or more substances in a volume produced by local chemical reactions and diffusion that causes the substances to distribute in the volume (Helms, 2018).

Particularly, for the multi compartmental modelling in skeletal muscle fibers is useful to consider the reaction diffusion equation in cylindrical coordinates, given the near-cylindrical shape of the skeletal muscle cells. Eq. 6 in cylindrical coordinates is expressed as:

$$\frac{dc}{dt} = D\left(\frac{d^2c}{dr^2} + \frac{1}{r}\frac{dc}{dr} + \frac{1}{r^2}\frac{d^2c}{d\Theta^2} + \frac{d^2c}{dx^2}\right) + f(x, r, \Theta, t) \tag{7}$$

for longitudinal distance *x*, radial distance *r* and axial rotation Θ.

2.3.2 Law of mass action

A great variety of chemical reactions take place both in the cytoplasm and within the intracellular compartments. The rate of change in a chemical reaction described by a kinetic diagram can be determined by a phenomenological law, the law of mass action. This law states that the rate of a chemical reaction is proportional to the product of the concentrations of the molecular species involved in the process (Fall, 2004). Suppose that a molecule A binds to a molecule B (substrate) to form the complex C (product) as is described in the following scheme:

$$A + B \underset{k_-}{\overset{k_+}{\rightleftharpoons}} C$$

where the molecules A and B are the substrates and C is the product, and k_+ and k_- are the forward and reverse rate constants of the reaction. According

to the law of mass action the reaction rate depends on the concentrations of the reacting species. The rate of this reaction is the rate of accumulation of the product, $d[C]/dt$. Since the quantity A is consumed by the forward reaction and produced by the reverse reaction, the rate of change of [A], and also of [B] is

$$\frac{d[A]}{dt} = - k_+[A][B] + k_-[C]. \quad (8)$$

The time evolution of the product [C] is the negative of this expression, given by:

$$\frac{d[C]}{dt} = k_+[A][B] - k_-[C]. \quad (9)$$

The dissociation constant of the reaction is defined by:

$$K_d = \frac{k_-}{k_+}. \quad (10)$$

At equilibrium, when the concentrations of the reactions do not change, we obtain:

$$K_d = \frac{[A][B]}{[C]}. \quad (11)$$

The inverse of K_d is called association constant K_a.

The total concentration of A, $[A]_T$, which can either be bound to B or free is given by:

$$[A]_T = [A] + [C] . \quad (12)$$

From Eq. 10 and 12 we obtain:

$$[A]_T = \frac{[C](K_d + [B])}{[B]}.$$

or

$$[C]=\frac{[A]_T[B]}{K_d+[B]}. \quad (13)$$

Then, [C] can be obtained from the value of K_d, [B] and $[A]_T$.

More complex binding reactions should include different types of molecular species. Also, more than a single molecule of a specific species can be required to form the product. For example, if we consider a reaction where two molecules of the same species A bind to one molecule of B to form the complex C,

$$2A + B \underset{k_-}{\overset{k_+}{\rightleftharpoons}} C$$

where, from the law of mass action, the rate of change of [A] is expressed as:

$$\frac{d[A]}{dt} = 2\left(-k_+[A]^2[B] + k_-[C]\right), \quad (14)$$

and in the case of [C], its rate of change over time is:

$$\frac{d[C]}{dt} = k_+[A]^2[B] - k_-[C] = -\frac{1}{2}\frac{d[A]}{dt}. \quad (15)$$

In the equilibrium the reaction rate is zero, $d[C]/dt=0$. From the Eq. 11 and 15 we obtain a dissociation constant

$$K_d=\frac{[A]^2[B]}{[C]}. \quad (16)$$

In a third case, when two reactions occur simultaneously, the molecule A reacts with B and D, separately, to form the complexes C and E:

$$A + B \underset{k_{1-}}{\overset{k_{1+}}{\rightleftharpoons}} C \qquad A + D \underset{k_{2-}}{\overset{k_{2+}}{\rightleftharpoons}} E$$

The dissociation constants $K_{1d}= k_{1-}/k_{1+}$ and $K_{2d}= k_{2-}/k_{2+}$ thus are:

$$K_{1d}=\frac{[A][B]}{[C]} \tag{17}$$

and

$$K_{2d}=\frac{[A][D]}{[E]}. \tag{18}$$

We also define $[A]_T$ as the total concentration of A, which can be bound to B, D and free,

$$[A]_T = [A] + [C] + [E] \tag{19}$$

From Eqs. 17, 18 and 19, [A], [C] and [E] are given by:

$$[A]=\frac{[A]_T K_{1d} K_{2d}}{[B]K_{2d}+K_{1d}K_{2d}+[D]K_{1d}}, \tag{20}$$

$$[C]=\frac{[A]_T [B] K_{2d}}{[B]K_{2d}+K_{1d}K_{2d}+[D]K_{1d}} \tag{21}$$

and

$$[E]=\frac{[A]_T [D] K_{1d}}{[B]K_{2d}+K_{1d}K_{2d}+[D]K_{1d}}. \tag{22}$$

[A] [C] and [E] can be obtained from $[A]_T$, [B], [D], K_{1d} and K_{2d}. This type of reaction can describe, for example, the binding of the PV molecules ([A]) to Ca^{2+} ([D]) and Mg^{2+}([E]) in the cytoplasm of the skeletal muscle fiber (Gillis et al., 1982).

2.3.3 The Michaelis-Menten model

Enzyme kinetics is the study of the chemical reactions that are catalyzed by enzymes. The Michaelis-Menten model describes enzymatic kinetic as a two-steps reaction in which an enzyme E converts a subtract S into a product P according to the following scheme of the reaction sequence:

$$E + S \underset{k_{1-}}{\overset{k_{1+}}{\rightleftharpoons}} ES \xrightarrow{k_{2+}} E + P$$

In the scheme, E reacts with S to form an intermediate complex ES, which then breaks down into the product P releasing E in the process. The constants k_{1+}, k_{1-} and k_{2+} represent the different rates of reaction. The step leading to product P in the scheme is assumed to be irreversible and E itself is not consumed or changed. From the law of mass action, we get that

$$\frac{d[ES]}{dt} = -k_{1+}[E][S] - (k_{-1} + k_{2+})[ES] \tag{23}$$

and

$$\frac{d[P]}{dt} = k_{2+}[ES] \tag{24}$$

If the reactions are sufficiently fast, it can be assumed that all species are in equilibrium. From Eq. 10 the dissociation constant is given by

$$K_d = [E][S]/[ES] \, . \tag{25}$$

Considering that the total [E], $[E]_T$, can be expressed as:

$$[E]_T = [E] + [ES] \tag{26}$$

Then from Eqs. 25 and 26

$$[ES]=\frac{[E]_T[S]}{K_d+[S]} \tag{27}$$

and from Eqs. 24 and 27 the flux or the rate of change of [P] is

$$\frac{d[P]}{dt}=k_{2+}\frac{[E]_T[S]}{K_d+[S]}$$

if $k_{2+}[E]_T = V_{max}$

$$\frac{d[P]}{dt}=V_{max}\frac{[S]}{K_d+[S]} \tag{28}$$

where V_{max} is the maximum rate of production of [P] and K_d is the half-maximum production rate. The Eq. 28 is called the Michaelis-Menten model. If the rate of change of P is given by the binding of a number *n* of molecules of S simultaneously, the rate of reaction can be expressed as:

$$\frac{d[P]}{dt}=V_{max}\frac{[S]^n}{K_d{}^n+[S]^n} \tag{29}$$

where *n* is known as the Hill coefficient.

2.3.4 Models of ECC in skeletal muscle fibers

Mathematical models of the Ca^{2+} movements have been developed to have a better understanding of the ECC mechanism during the activation of skeletal muscle fibers. Cannell and Allen (1984) proposed the first multi compartment model to describe the diffusion and reaction of Ca^{2+} in frog skeletal muscle fibers. Subsequent models have been developed over the time by the integration of information gathered on ECC. An extension to this model was developed by Holly and Poledna (1989) to include terms for Ca^{2+} uptake by the SERCA (Hollý & Poledna, 1989).

In the models then proposed by Baylor and Hollingworth, the role of ATP was considered and also an accurate description of the mammalian skeletal

muscle, discriminating between fast and slow fibers (S M Baylor & Hollingworth, 1998; Stephen M. Baylor & Hollingworth, 2007b; Stephen M Baylor & Hollingworth, 2012; Stephen Hollingworth et al., 2012).

A model developed by Liu and Olson (2015) focused on modelling the membrane ion channels, with a detailed description of the Ca^{2+} release from the SR, its dependency with the membrane potential and its inactivation when the Ca^{2+} concentration is high in the cytoplasm (Liu & Olson, 2015).

In a more recent work by Marcucci and coworkers (2018), the Ca^{2+} flux through the mitochondria is included for the first time. Measurements of Ca^{2+} transients in the mitochondria support the theorical results (Marcucci et al., 2018).

In general, the Ca^{2+} reaction-diffusion simulations of skeletal muscle fibers, divide the sarcomere into a 3-dimensional array of smaller compartments, and use a series of ordinary differential equations (ODE) to represent the diffusion, binding, and pumping reactions that occur within and between the compartments.

Together, these sarcomere simulations have proven to be valuable tools for the identification of the large localized concentration gradients that exist during muscle activation, the importance of Ca^{2+} buffers, and for identifying experimental errors that can arise when using Ca^{2+} indicators (Stephen M. Baylor & Hollingworth, 2011). However, some limitations are still found in above quoted models, such as: i) they are based on experimental results performed without a reliable identification of the fiber type used; ii) they do not take into account all the known mechanisms leading to Ca^{2+} disappearance of the fiber type used; iii) they derive from experiments using intracellular Ca^{2+} dyes with slower Ca^{2+} kinetics than the Ca^{2+} buffers and Ca^{2+} uptake

kinetics which in turn do not reliably track the Ca^{2+} transients in skeletal muscle fibers.

2.3.5 Conversion of fluorescent intensity to [Ca^{2+}]

Measurements of Ca^{2+} transients obtained from non-ratiometric fluorescent indicators such as Fluo-4 can be calibrated and expressed in terms of [Ca^{2+}] (Caputo et al., 1994; Grynkiewicz et al., 1985). Assuming that the reactions of the fluorescent indicator with Ca^{2+} can be described as the following reversible reactions:

$$Ca^{2+} + Dye \underset{k_-}{\overset{k_+}{\rightleftharpoons}} CaDye$$

where the Dye and CaDye represent the Ca^{2+}-free and Ca^{2+}-bound forms of the indicator. From Eq. 10 we obtain the following expression:

$$[Ca^{2+}] = \frac{K_d[CaDye]}{[Dye]}, \tag{30}$$

and the total [Dye] is given by:

$$[Dye]_T = [Dye] + [CaDye]\ . \tag{31}$$

The fluorescent intensity F can be described as (Grynkiewicz et al., 1985):

$$F = S_f\,[Dye] + S_b[CaDye] \tag{32}$$

where S_f and S_b are proportionality coefficients of the indicator in free and bound form. The value of F varies between two limits, the minimum and maximum fluorescence (F_{min} and F_{max}). The fluorescence achieves the minimum value when [CaDye]=0 and the maximum when [Dye]=0, so the [CaDye] is maximal. Thus, we have that:

$$F_{min} = S_f\,[\mathrm{Dye}]_T \tag{33}$$

and

$$F_{max} = S_b\,[\mathrm{Dye}]_T \tag{34}$$

From Eqs. 30, 31, 33 and 34 we get that

$$[\mathrm{Dye}] = \frac{F_{max} - F}{S_b - S_f} \tag{35}$$

and

$$[\mathrm{CaDye}] = \frac{F - F_{min}}{S_b - S_f} \tag{36}$$

Replacing Eqs. 35 and 36 in 30 we obtain the following expression:

$$[Ca^{2+}] = K_d \frac{F - F_{min}}{F_{max} - F}, \tag{37}$$

which allows us to obtain the $[Ca^{2+}]$ from measurements of F by determining the values of K_d, F_{max} and F_{min}. This model was proposed by Grynkiewicz et al. (1985) and has been widely used previously (Stephen M. Baylor & Hollingworth, 2007b; Delbono & Stefani, 1993; Stephen Hollingworth et al., 2012). Under dynamic conditions, such as during a Ca^{2+} transient, the rate of change of [CaDye] over time, $d[\mathrm{CaDye}]/dt$, can be obtained from Eq. 9

$$\frac{d[\mathrm{CaDye}]}{dt} = k_+[Ca^{2+}][\mathrm{Dye}] - k_-[\mathrm{CaDye}]. \tag{38}$$

Replacing Eqs. 35 and 36 in 38 we get that the rate of change of fluorescence is:

$$\frac{dF}{dt} = k_+[Ca^{2+}](F_{max} - F) - k_-(F - F_{min}), \tag{39}$$

and considering that: $F = F_{rest} + \Delta F$, where F_{rest} is the resting fluorescence and ΔF the change of fluorescence, the Eq. 38 can be rewritten as:

$$[Ca^{2+}] = \frac{k_{-}(F_{rest} + \Delta F - F_{min}) + dF/dt}{k_{+}(F_{max} - F_{rest} + \Delta F)}, \quad (40)$$

From the Eq. 37 we obtain that at rest:

$$F_{rest} - F_{min} = k_{+} [Ca^{2+}]_R (F_{max} - F_{rest}) / k_{-}. \quad (41)$$

Replacing Eqs. 41 in 40 we obtain the following expression:

$$[Ca^{2+}] = \frac{[Ca^{2+}]_R (F_{max} - F_{rest}) k_{+} + \Delta F k_{-} + dF/dt}{k_{+}(F_{max} - F_{rest} + \Delta F)}, \quad (42)$$

which allows us to obtain the $[Ca^{2+}]$ from measurements of F by determining the values of k_{-}, k_{+}, F_{max}, F_{rest} and $[Ca^{2+}]_R$. This model was presented by Caputo et al. (1994) and unlike the model of Grynkiewicz et al. (1985) it does not requiere the F_{min} measurement.

2.3.6 Objectives

General objective

To propose a mathematical model to simulate Ca^{2+} movements during ECC in different fiber types of mammalian skeletal muscle fibers.

Specific objectives

- To propose a multi-compartment model of the Ca^{2+} movements based on kinetic parameters associated with the four fiber types (I, IIA, IIX and IIB) and the molecular machinery involved in the mammalian ECC.
- To include in the mathematical model the Na^{+}/Ca^{2+} exchanger and the mitochondria.
- To compare the role of the release and reuptake mechanisms during single Ca^{2+} transients.

Chapter 3

Methods

In this chapter we present the Ca^{2+} transients measurements that we used as input of the model to obtain the simulated results. We also propose a model to describe the [Ca^{2+}] changes and we present the simulated values that change according to each fiber type.

3.1 Measurements of Δ[Ca^{2+}] used for the simulations

The experimental data used for the simulations were obtained with a calibration that allows converting the fluorescence signals generated with the Mag-Fluo-4 AM fluorescent indicator into [Ca^{2+}]. The measurements of *F* during single Ca^{2+} transients of fiber types I, IIA, IIX/D and IIB were taken from Calderón et al. (2010), and during tetanic Ca^{2+} transients of MT-I and MT-II produced by trains of APs with different durations and at 100 Hz were taken from Calderon et al. (2014).

Recent measurements, carried out by our group, of the properties of Ca^{2+} and Mg^{2+} fluorescent dye Mag-Fluo-4 suggest that in the Ca^{2+}-Mag-Fluo-4 reaction two molecules of the fluorescent indicator bind to one Ca^{2+} (Milán et al. in *prep.*), which is in disagreement with the initial assumption used in the models of Grynkiewicz et al. (1985) and Caputo et al. (1994) for other Ca^{2+} dyes. Assuming that the reactions of the fluorescent indicator with Ca^{2+} can be described as the following reversible reactions:

$$D + Ca^{2+} + D \underset{k_r}{\overset{k_f}{\rightleftharpoons}} CaD_2$$

The steady-state binding equation associated with the scheme is:

$$[Ca^{2+}][D]^2 = K_d[CaD_2], \quad (43)$$

where [Ca] and [D] are the concentrations of free Ca^{2+} and free dye, $[CaD_2]$ is the concentration of the Ca^{2+}-dye complex and K_d is the dissociation constant of the reaction. The total dye concentration $[D]_T$ is given by

$$[D]_T = [D] + 2[CaD_2]. \quad (44)$$

The experimental fluorescent intensity *F* can be described as (Grynkiewicz et al., 1985):

$$F = S_f [D] + S_b[CaD_2] , \quad (45)$$

where S_f and S_b are proportionality coefficients of the indicator in free and bound form. From Eq. 44 and 45 we get:

$$F = S_f[D] + \frac{S_b}{2}([D]_T - [D]) . \quad (46)$$

The value of *F* varies between two limits, the minimum and maximum fluorescence (F_{min} and F_{max}). The fluorescence achieves the minimum value when no indicator molecule is bound to Ca^{2+} ($[CaD_2]=0$ and $[D]= [D_T]$) and the maximum when all is bound ($2[CaD_2]= [D_T]$ and $[D]=0$)

$$F_{max} = \frac{S_b}{2}[D]_T \quad (47)$$

and

$$F_{min} = S_f[D]_T \quad (48)$$

From Eqs. 46 and 48 we get that the fluorescent signal produced by the bound dye is:

$$F\text{-}F_{min} = 2\left(\frac{S_b}{2}\text{-}S_f\right)[CaD_2]\,, \tag{49}$$

With an analogue approach, from Eqs. 46 and 47, the relationship between the reverse of fluorescence (F_{max}-F) and the free dye is:

$$F_{max}\text{-}F = \left(\frac{S_b}{2}\text{-}S_f\right)[D] \tag{50}$$

And from Eqs. 47 and 48:

$$F_{max}\text{-}F_{min} = \left(\frac{S_b}{2}\text{-}S_f\right)[D]_T\,. \tag{51}$$

Replacing Eqs. 49, 50 and 51 in 43

$$\left[Ca^{2+}\right] = \frac{K_d}{[D]_T}\frac{(F\text{-}F_{min})(F_{max}\text{-}F_{min})}{2(F_{max}\text{-}F)^2}\,. \tag{52}$$

which allows us to obtain the $[Ca^{2+}]$ from measurements of F by determining the values of K_d, F_{max}, F_{min} and $[D]_T$.

The fluorescence signals are converted into measurements of $[Ca^{2+}]$ with Eq. 52. Where F_{min} is taken as 0.14, F_{max} as 150.889 and $[D]_T$=246.54 µM (Milán et al. 2020, *in prep*.). In order to estimate the K_d we use a Mag-Fluo-4 calibration curve in situ which relates the $[Ca^{2+}]$ to F. We consider Eq. 52 when $F = (F_{max}+F_{min})/2$:

$$\frac{K_d}{[D]_T} = \left[Ca^{2+}\right]\,. \tag{53}$$

So, $K_d/[D]_T$ can be estimated from the value obtained for the $[Ca^{2+}]$ when $F = (F_{max}+F_{min})/2$ in the calibration curve (Fig. 6).

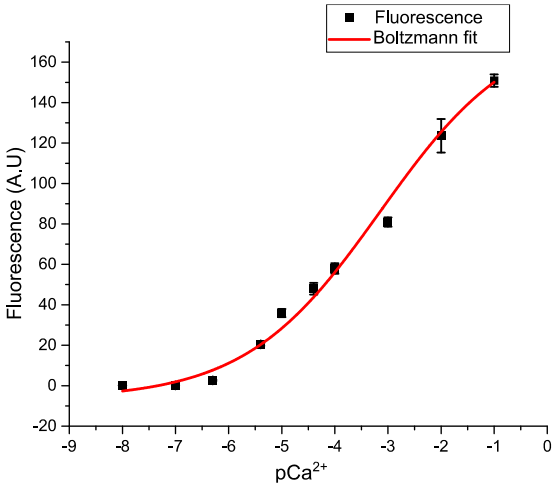

Model	Boltzmann
Equation	y = A2 + (A1-A2)/ (1 + exp((x-x0)/dx))
Plot	Fluorescence
A1	-6,62471 ± 7,27263
A2	179,18418 ± 37,53544
x0	-3,14202 ± 0,65968
dx	1,27188 ± 0,47558
Reduced Chi-Sq	0,18899
R-Square (COD)	0,99982
Adj. R-Square	0,99972

Fig. 6. Ca^{2+}-Mag-Fluo-4 calibration curve *in situ*. Fluorescence intensity (in arbitrary units) was recorded with a photomultiplier in fibers from *flexor digitorum brevis* of mouse loaded with 6 µM extracellular Mag-Fluo-4 and was plotted against the pCa ($-\log_{10}([Ca^{2+}])$) reached in the cytoplasm after different experimental treatments. The curve is fitted by the Boltzmann equation for K_d estimation. The parameter x0 of -3.14202 is equivalent to the pCa value at half response (when $F = (F_{max}+F_{min})/2$). Taken from Milán et al., (2021).

3.2 Model of Ca^{2+} movements

3.2.1 Geometry of the model

Given the extensively reported regularity and the radial symmetry of the muscle fiber, we describe half sarcomere (Fig. 7), from line *m* to line *z*, assuming a cylindrical geometry with a radius between 0.5 m and 0.7 µm (Hirose et al., 1994a; Hodge et al., 1954) and a length of 1 µm (Bolaños et al., 2008; Calderón et al., 2009). The cylinder was divided into a set of compartments of equal volume, with n radial divisions and m longitudinal divisions. We assumed that the number of radial and longitudinal subdivisions were n=5 and m=10 (i.e. 50 compartments), since simulations

using finer divisions (up to 300 compartments) show similar results (Marcucci et al., 2018). Fig. 7 shows a schematic representation of the compartmentalized geometry of the model for typical slow-twitch (Fig. 7A) and fast-twitch (Fig. 7B) muscle fibers. The set of values used in the simulation for the geometry of the model along with the other parameters are presented in the Table 1.

The occupancy of the mitochondria relative to the cytoplasm, referred to as MITO volume, for the fast-twitch fibers ranges from 2.2% (in gastrocnemius fibers of rat) to 8% (in EDL fibers of mouse) (Eisenberg, 2011a). For the slow-twitch muscle fibers it ranges from 5.9% (in soleus of rat) (Eisenberg, 2011a) to 15% (in soleus of mouse) (Chen et al., 2001). The relative occupancy of the SR is also different for fast and slow-twitch and up to 3.2 times higher in fast-twitch fibers. For example, the SR volume in rats varies from 5.5% (soleus) to 9.3% (EDL), and in mice from 2.9% (soleus) to 5.5% (EDL) (Eisenberg, 2011a).

Consequently, we took the average values 5.1% and 7.4% as the fraction volume occupied by MITO and SR, respectively, in fast-twitch muscle fibers. The cytoplasmic water volume is thus 87.5%. The corresponding average values for slow-twitch muscle fibers were 10.45% (MITO) and 4.2% (SR) leaving a cytoplasmic water volume of 85.4%.

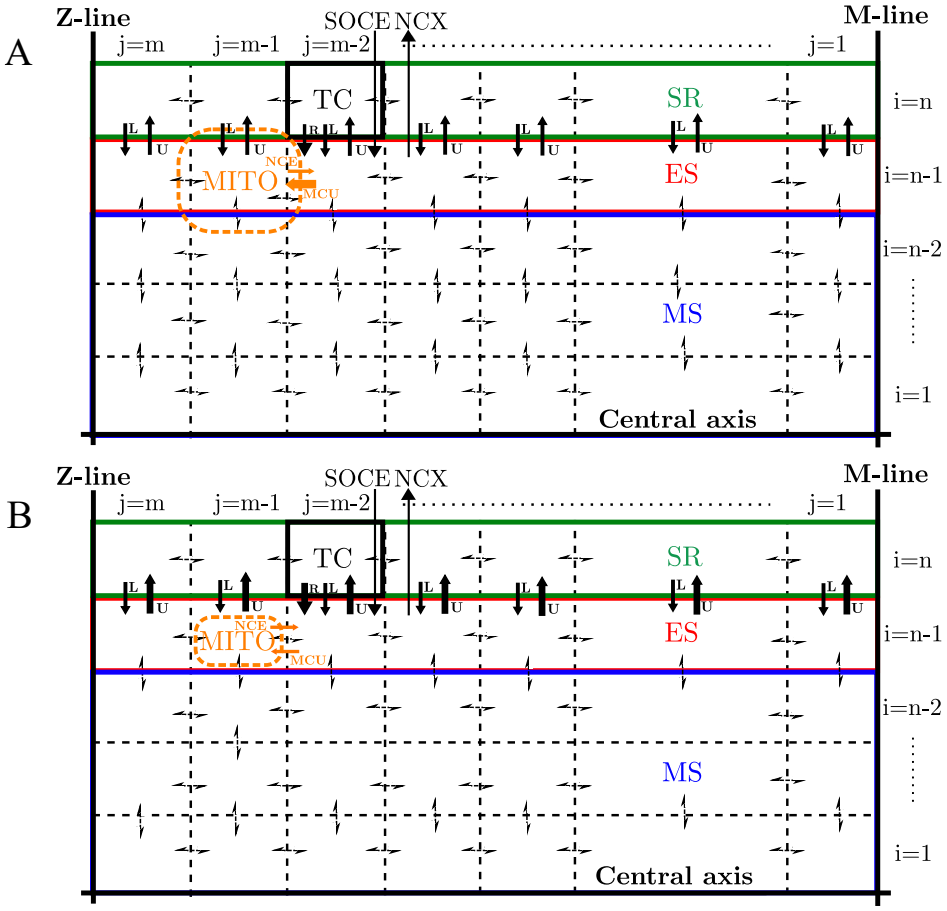

Fig. 7. Schematic representation of geometry and Ca^{2+} fluxes in the model for slow-twitch (A) and fast-twitch muscle fibers (B). The symmetric of half sarcomere is divided into *m* longitudinal sections and *n* radial sections (indicated with the discrete variables *i* and *j*). The myofibrillar space (MS) occupies the radial compartments from $i=1$ to $i=n-2$. Row $i=n-1$ is occupied by the extramiofibrillar space (ES) and in i=n is the sarcoplasmic reticulum (SR). The mitochondria (MITO) are close but external to the ES. In both cases (fast and slow) Ca^{2+} is free to diffuse along these compartments and into the MS, ES and SR (dashed arrows). Ca^{2+} movements between the SR and the ES are determined by the release (R) from the TC, the Ca^{2+} uptake (U) from the ES by the SERCA pump and a small constant Ca^{2+} leak (L) from each SR element (which is small and constant). The arrows representing the fluxes through the compartments

have differences in their thickness that indicate a quantitative change in the simulated values.

Since the concentrations of the muscle proteins are frequently reported in units of mol/kg whole muscle, we estimate a correction factor to convert from mol/kg whole muscle to mol/kg cytoplasmic H_2O. Following the procedure proposed in Baylor et al. (1983), with the assumed fractional volume occupied by the SR and the MITO in our model, a factor of 0.58 (g cytoplasmic H_2O)/(g whole muscle) is obtained for fast fibers and 0.56 (g cytoplasmic H_2O)/(g whole muscle) in slow fibers.

3.2.2 Diffusion and reaction of Ca^{2+}

The diffusion and binding of a chemical species, in this case the Ca^{2+} in a homogeneous isotropic medium with cylindrical geometry, is described with the reaction diffusion equation in cylindrical coordinates, which is expressed as

$$\frac{\partial[\mathrm{Ca}^{2+}]}{\partial t} = \frac{1}{r}\frac{\partial(D\, r\, [\mathrm{Ca}^{2+}])}{\partial r} + \frac{\partial(D\, [\mathrm{Ca}^{2+}])}{\partial x} - F([\mathrm{Ca}^{2+}], S)\ , \qquad (54)$$

where $[Ca^{2+}]$ is the concentration of Ca^{2+}, D is the diffusion coefficient, x is the longitudinal coordinate, r is the radial coordinate and F accounts for local reactions with binding sites S.

By considering circumferential symmetry, $[Ca^{2+}]$ does not depend on axial rotation. So, Eq. 54 is a particular case of Eq. 7. We then used the approach proposed in Crank (1975) that was also applied in previous models (Cannell & Allen, 1984; Marcucci et al., 2018),

$$\frac{\partial[\mathrm{Ca}^{2+}]}{\partial t} = \frac{4D\mathrm{n}}{\mathrm{R}^2}\left[i\left([\mathrm{Ca}^{2+}]_{i+1,\,j} - [\mathrm{Ca}^{2+}]_{i,\,j}\right) - (i-1)\left([\mathrm{Ca}^{2+}]_{i,\,j} - [\mathrm{Ca}^{2+}]_{i-1,\,j}\right)\right] \qquad (55)$$

$$+D\left(\frac{\mathrm{m}}{\mathrm{L}}\right)^{2}\left([Ca^{2+}]_{i,j+1}-2[Ca^{2+}]_{i,j}+[Ca^{2+}]_{i,j-1}\right)-F\left([Ca^{2+}]_{i,j}, S\right),$$

where R and L are the radius and length of the cylindrical geometry, and *m* and *n* are the number of radial and longitudinal divisions. The diffusion coefficient for cytoplasmic free Ca^{2+} was taken as 0.7 μm²/ms (J. H. Wang, 1953). This approach allows to numerically solve the set of ODE that describes the changes in $[Ca^{2+}]$. For that aim, the *ode15s* solver in MATLAB 2019b was used.

3.2.3 Ca^{2+} binding to the skeletal muscle buffers

The local reactions of Ca^{2+} with the other chemical species present in each compartment are described by the law of mass action, with the following general expression:

$$F([Ca^{2+}], S) = k_{-}[SCa^{2+}]-k_{+}[Ca^{2+}][S], \quad (56)$$

where S are the binding sites, k_{+} is the binding rate constant and k_{-} is the separation rate constant.

The interactions of Ca^{2+} and Mg^{2+} with the binding sites are described with different types of reversible reactions (Fig. 8). The reactions with ATP, Trop, mitochondrial buffers (B) and calsequestrin (CSQ) are described as single reversible reaction (Fig. 8a). Since Mg^{2+} competes with Ca^{2+} for the PV, their interaction are described with two simultaneous reversible reactions (Fig. 8b). Also as described in (Milán et al., 2021), in the reaction between Ca^{2+} and Mag-Fluo-4, two molecules of the fluorescent indicator bind to one of Ca^{2+} (Fig. 8c).

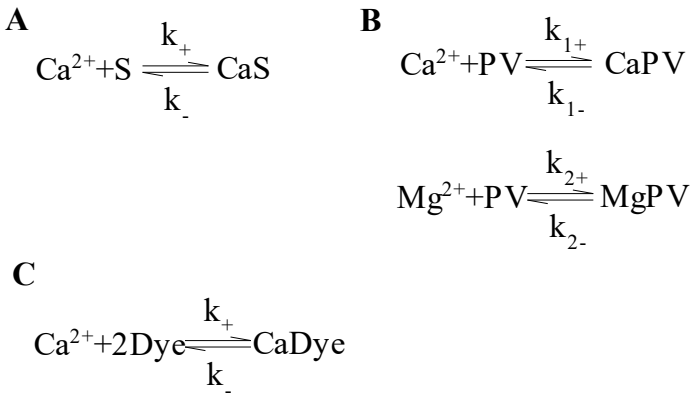

Fig. 8. Simplified reaction schemes for ATP, Trop, mitochondrial buffers and calsequestrin (A), parvalbumin (B) and the fluorescent indicator Mag-Fluo-4 AM (C).

The Trop content in skeletal muscle is 0.07 mmol/kg (Ebashi et al., 1969), and we assume that it is uniformly distributed through the MS. Using 1/0.58 and 1/0.56 as factors for converting mol/kg whole muscle to mol/kg of cytoplasmic H_2O, the concentration of Trop is 120 µM and 125 µM. Consequently, we used 240 µM and 250 µM of low affinity Ca^{2+} binding for fast and for slow-twitch fibers, respectively. The reaction between the Trop sites and Ca^{2+} was modeled with an *off-rate* constant of 23.0 s^{-1} (Robertson et al., 1981), and an *on-rate* constant of 1.15×10^8 M^{-1} s^{-1} obtained with a binding constant of 5×10^6 M^{-1} (Potter & Gergely, 1975).

The PV content in the fastest fibers of mouse (IIB) can be as high as 4.9 g/kg whole muscle (Heizmann et al., 1982). Assuming a molecular weight of 12 kDa and the previously estimated conversion factor, [PV] in the IIB type is 1500 µM. Fibers type I have 200-300 times less [PV] (Leberer & Pette, 1986), leading to 5-7 µM. Fibers IIA have PV concentrations closer to fibers type I than type II (Füchtbauer et al., 1991; Leberer & Pette, 1986), giving values from 7 to 155 µM. The *off-rate* constant for Ca^{2+} was taken as 1.01 s^{-1}

(Donaldson et al., 1978), and the *on-rate* constant as 2.5×10^{8} $M^{-1}s^{-1}$ obtained with a binding constant of 2.5×10^{8} M^{-1} (Robertson et al., 1981) The assumed Mg^{2+} *off-rate* constant was 6 s^{-1} (Donaldson et al., 1978), and the *on-rate* constant 6.6×10^{4} $M^{-1}s^{-1}$ (Robertson et al., 1981). The similarity of the values of the on and off rate for Mg^{2+} and Ca^{2+} agree with the assumption that both compete to bind to PV. A uniform distribution of the PV through the MS and the ES was assumed.

The ATP concentration at rest is about 1.6-1.9 times higher in fast than in slow-twitch muscle fibers of mammals, including murine models (Hintz et al., 1982; Kushmerick et al., 1992; Racay et al., 2006). In rat fibers the ATP content is 18.3 mmol/kg dry wt in slow and 30.3 mmol/kg dry wt in fast fibers. Assuming a ratio around 5 between mmol/kg dry wt and mM units (Schiaffino & Reggiani, 2011), we obtain a concentration of 3.66 mM for slow fibers and 6.06 mM for fast fibers. In mouse, measurements of the ATP content has ranged from 4.3 to 8 mM for fast fibers from 2.2 to 5 mM for slow fibers (Kushmerick et al., 1992; Racay et al., 2006). We assumed that the ATP reaction with Ca^{2+} has *off-rate* and *on-rate* constants of 3×10^{3} s^{-1} and 0.1364×10^{8} M^{-1} s^{-1} , respectively (S M Baylor & Hollingworth, 1998). We also assumed that the ATP is distributed uniformly through the MS and the ES.

CSQ is a Ca^{2+} binding protein that is predominantly located in the terminal cisternae (TC) of the SR (Jorgensen et al., 1979), with two isoforms (CSQ1 and CSQ2) depending on the fiber type (Damiani & Margreth, 1994). Both isoforms can be found in slow fibers, whereas only CSQ1 is expressed in fast fibers. We assumed 2.9 mM sites on CSQ1 for fast fibers and, for slow fibers 1.07 mM (0.77 mM and 0.3 mM sites on CSQ1 and CSQ2, respectively)

(Murphy et al., 2009). The *on-rate* constant 3 10^{-3} μM^{-1} s^{-1}, and the *off-rate* value is 3 ms^{-1} (Westerblad & Allen, 1994).

As explained before, the reaction of the Mag-Fluo-4 with Ca^{2+} is reversible and their stoichiometry is 2:1 (i.e. two molecules of Mag-Fluo-4 for every one of Ca^{2+}). The assumed *off-rate* constant is 8.72 10^5 s^{-1}, and the *on-rate* constant of 4.9 M^{-2} s^{-1} is obtained with a binding constant of 1.5977 10^5 μM^2 (Milán et al. 2020).

The occupancy fraction of the binding sites at equilibrium was calculated from the K_d values of each buffer, the total binding sites and the assumed values of free [Ca^{2+}] and [Mg^{2+}] at rest of 106 nM, and 0.78 mM, respectively (Westerblad & Allen, 1992; Williams et al., 1990). In the SR compartment we assumed a [Ca^{2+}] at rest of 1.01 mM for fast fibers and 1.14 mM for slow fibers (Fryer & Stephenson, 1996). The concentration of Ca^{2+} and Mg^{2+} bound to each buffer is determined by the law of mass action. Each case was described in section 2.3.2 and the expression that relates dissociation constants to the concentration of chemical species were used to estimate the occupation fraction of the binging sites by Ca^{2+} (also Mg^{2+} in the case of PV).

3.2.4 Reuptake rate of Ca^{2+} for SERCA

The reuptake of Ca^{2+} by SERCA is described by the Michaelis-Menten kinetics, which relates the reuptake rate to the SR, with the Ca^{2+} available in the cytoplasm by the following expression:

$$J_{SERCA} = V_{SERCA} \frac{[Ca^{2+}]^{h_{SERCA}}}{[Ca^{2+}]^{h_{SERCA}} + K_{SERCA}^{h_{SERCA}}} \quad (57)$$

where V_{SERCA} represents the maximum reuptake rate, reached at a saturating $[Ca^{2+}]$, K_{SERCA} is the $[Ca^{2+}]$ at which the reaction rate is half of V_{SERCA} and h_{SERCA} is the Hill coefficient.

The SERCA 1a isoform is expressed in fast-twitch muscle fiber from adult mammalian, whereas in slow-twitch muscle fiber from adult mammalian the isoform SERCA 2a is expressed predominantly (Periasamy & Kalyanasundaram, 2007).

The K_{SERCA} and the maximal Ca^{2+} uptake per unit of pump mass of the 1 and 2a SERCA isoforms are similar (Campbell et al., 1991; Lytton et al., 1992). Thus, the V_{SERCA} for the different fiber types depends mainly on the different amount of the pump present in the studied volume. Given that the fast-twitch fibers have between 2 and 6 fold higher concentration of SERCA than the slow-twitch fibers (Ferguson & Franzini-Armstrong, 1988; Leberer & Pette, 1986), the V_{SERCA} values assumed for the present work ranged from 0.831 μM ms^{-1} for fiber types IIX/D and IIB (Stephen M. Baylor & Hollingworth, 2007b), to 0.415 μM ms^{-1} and 0.138 μM ms^{-1} for fiber types IIA and I, respectively.

3.2.5 Mitochondrial MCU inflow and NCE outflow

The equation that describes the change of Ca^{2+} concentration in the mitochondria is

$$\frac{\partial [Ca^{2+}]_{mito}}{\partial t} = J_{MCU}([Ca^{2+}]_{cyto}) - J_{NCE}([Ca^{2+}]_{mito},[Ca^{2+}]_{cyto}) - F([Ca^{2+}]_{mito}, B) \quad (58)$$

where J_{MCU} is the inflow through the mitochondrial Ca^{2+} uniporter (MCU) and J_{NCE} the outflow through the mitochondrial Na^{2+}/Ca^{2+} exchanger (NCE). Fig. 9 shows a simplified schematic representation of Ca^{2+} movement in mitochondria. The description of these two flows is based on previous models

of Ca^{2+} movement in mitochondria of cardiac and skeletal muscle fibers (Dash & Beard, 2008b; Marcucci et al., 2018; Wüst et al., 2017). The mitochondrial buffers B are assumed to be uniformly distributed and to react with Ca^{2+}. We took 2 µM of binding sites, which react with Ca^{2+} with binding and unbinding rate constants of 0.8 $\mu M^{-1}s^{-1}$ and 0.192 s^{-1} (Marcucci et al., 2018).

We also assume J_{MCU} as a saturable first-order transporter independent of the internal $[Ca^{2+}]_{MITO}$:

$$J_{MCU}=V_{MCU}\frac{[Ca^{2+}]^{h_{MCU}}}{[Ca^{2+}]^{h_{MCU}}+k_{MCU}^{h_{MCU}}} \quad (59)$$

where V_{MCU} is the maximum flux rate, $[Ca^{2+}]_{cyto}$ is the Ca^{2+} concentration in the sub-compartment of ES where the mitochondrion resides in and k_{MCU} is the $[Ca^{2+}]$ where the "pump*"* rate is half-maximum.

We estimated a maximum rate of the Ca^{2+} uptake, for both slow-and fast-twitch muscle fibers, following Baylor et al. (2007) and Hollingworth et al. (2012). We took 145 and 65 nmol Ca^{2+} (mg protein)$^{-1}$ min^{-1} for slow and fast-twitch muscle fiber, respectively. Given a mitochondrial volume by protein content of 2.63 mm^3/mg in soleus and 2.58 mm^3/mg in gracilis (Schwerzmann et al., 1989), we obtain 918 nmol Ca^{2+}/cm^3 of mitochondria per second in slow fibers and 420 nmol Ca^{2+}/cm^3 of mitochondria per second of fast fibers. Additionally, by considering the assumed values for fraction volume occupied by the MITO and the SR, maximum rates of Ca^{2+} uptake of 111.8 µM/s in slow fibers and 24.5 µM/s in fast fibers were obtained.

The kinetics of the MCU Ca^{2+} flux was modeled with a k_{MCU} of 1.97 µM in slow fibers and 1.2 µM in fast fibers, and the Hill coefficients assumed were 2 and 2.5 (Sembrowich et al., 1985).

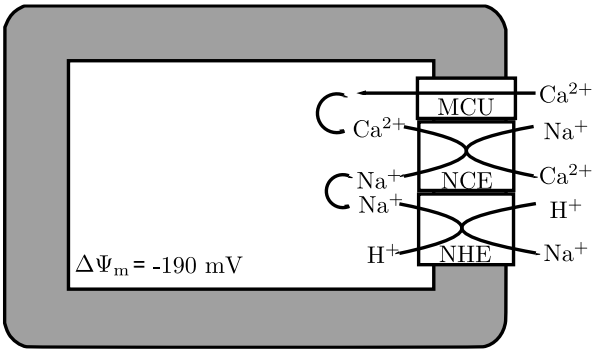

Fig. 9. Simplified model of Ca^{2+} flow in mitochondria. Typical Ca^{2+} inflow fluxes are through the MCU, driven by the negative potential inside the mitochondria, while typical outflow fluxes are through the NCE.

The flux through the NCE was modeled assuming a stoichiometry of 3:1 and described with the following expression (Dash & Beard, 2008b):

$$J_{NCE}=V_{NCE}\left(\frac{e^{\frac{0.5\Delta\Psi_m F}{RT}}\frac{[Na^+]_x^3[Ca^{2+}]_m}{k_{Na}^3 k_{Ca}}-e^{-\frac{0.5\Delta\Psi_m F}{RT}}\frac{[Na^+]_x^3[Ca^{2+}]_x}{k_{Na}^3 k_{Ca}}}{1+\frac{[Na^+]_x^3}{k_{Na}^3}+\frac{[Ca^{2+}]_m}{k_{Ca}}+\frac{[Na^+]_x^3[Ca^{2+}]_m}{k_{Na}^3 k_{Ca}}+\frac{[Na^+]_m^3}{k_{Na}^3}+\frac{[Ca^{2+}]_x}{k_{Ca}}+\frac{[Na^+]_m^3[Ca^{2+}]_x}{k_{Na}^3 k_{Ca}}}\right) \quad (60)$$

where $\Delta\Psi_m$ is the mitochondrial membrane potential, V_{NCE} is the NCE activity and $k_{Ca,NCE}$ and $k_{Na,NCE}$ are the Michaelis–Menten constants for the Ca^{2+} and Na^{2+} binding to the NCE. *F*, *R* and *T* denotes the Faraday constant, ideal gas constant and temperature, respectively. The equation considers a chemical and an electrical behavior on which the flow of Ca^{2+} in the mitochondria depends.

We assumed a $k_{Ca,NCE}$ of 1.1 µM and a $k_{Na,NCE}$ of 8.2 mM, which fitted the experimental curve of $[Ca^{2+}]_{MITO}$ performed by Marcucci and coworkers (2018). The assumed $\Delta\Psi_m$ was 190 mV. V_{NCE} was modulated to reproduce the speed of the $[Ca^{2+}]_{MITO}$ decay phase, completed in a period of about 100

ms and measured in skeletal muscle fibers during a single twitch, as in Rudolf et al. (2004).

3.2.6 Ca^{2+} flux through NCX

Since the NCX is predominantly located in the T-tubules membrane (Sacchetto et al., 1996), we assumed that it senses the $[Ca^{2+}]$ in the cytoplasm compartment closest to the T-tubule membrane, located at $i=n$-1 and $j=m$-3, and that removes the Ca^{2+} to the extracellular space. To describe the sarcolemmal NCX, the same expression for the NCE, with stoichiometry of 3:1 was used, although with different simulated values.

The rate of Ca^{2+} transport of the SERCA in membrane vesicles was reported as about 10 nmol mg^{-1} min^{-1} (Hidalgo et al., 1986), while for the NCX1 and NCX3 isoforms, 14 and 13 nmol mg^{-1} min^{-1} were reported (Linck et al., 1998). The NCX1 isoform predominates in slow-twitch and NCX3 in fast-twitch skeletal muscle fibers (Fraysse et al., 2001; Hudecova et al., 2004). Assuming that the maximum transfer rate for the NCX is 0.4 and 0.3 times higher than for the SERCA, the assumed V_{NCX} was 1.163 µM/ms and 0.179 µM/ms in fast and slow fibers, respectively. For $k_{Ca,NCX}$ and $k_{Na,NCX}$, we respectively took values of 140 µM and 14 mM in fast fibers, and 130 µM and 11 mM in slow fibers (Linck et al., 1998). The assumed sarcolemmal membrane potential was 80 mV.

3.2.7 The effect of store-operated Ca^{2+} entry (SOCE)

We described the flux, J_{SOCE}, as a fraction, P_{SOCE}, of a given maximum value, V_{SOCE} as $J_{SOCE}= V_{SOCE}\, P_{SOCE}$ (Croisier et al., 2013). As said, P_{SOCE} change as a function of the $[Ca^{2+}]$ in the SR, which can be described by the function:

$$P_{SOCE}=\frac{K_{SOCE}^{h_{SOCE}}}{[Ca^{2+}]_{SR}^{h_{SOCE}}+K_{SOCE}^{h_{SOCE}}} \quad (6)$$

where K_{SOCE} and h_{SOCE} are the Ca^{2+} dissociation constant of STIM1 (0.35 mM) and the Hill coefficient (4.7) (Koenig et al., 2019). We assumed that the V_{SOCE} in the fastest IIB fibers achieved up to 35 μM s^{-1} (Koenig et al., 2019). Lower values were used for IIX, IIA and I fibers.

3.3 Estimation of the release rate of Ca^{2+}

3.3.1 Single compartment estimation

The release rate of Ca^{2+} from the SR can be estimated from measurements of cytoplasmic Ca^{2+} transients obtained with a fluorescent indicator, which in this case is the Mag-Fluo-4 AM, used as an input of the models of the Ca^{2+} movements (S M Baylor & Hollingworth, 2003b). Since spatially averaged $[Ca^{2+}]$ in the cytoplasm was used, it was also assumed that Ca^{2+} and other chemical species that react with Ca^{2+} are uniformly distributed in the cytoplasm. Thus, the cytoplasm is described with a single-compartment model to estimate the release rate of Ca^{2+}. The time derivative of the total Ca^{2+} concentration in the cytoplasm, $d[Ca_T]/dt$, is given by the sum of the inflows and outflows, J_{Rec}, through the membrane. Increases in $d[Ca_T]/dt$ are caused by the release rate of Ca^{2+} and falls are due to the J_{Rec}. Therefore, from the sum of $d[Ca_T]/dt$ and J_{Rec}, it is possible to obtain the release rate of Ca^{2+}.

The $d[Ca_T]/dt$ can be determined by the sum of the change in the concentration of free Ca^{2+}, the Ca^{2+} coupled to the buffers in the cytoplasm (Trop, PV and ATP) and to the fluorescent indicator that is used during the measurement (Dye). $[Ca^{2+}]$ is determined by the measurement of the

fluorescence signal generated by an electrical stimulus; whilst [CaDye], [CaTrop], [CaPV] and [CaATP] are estimated with the available information on the concentration and the speed with which these proteins react with Ca^{2+} for different fiber types, with the law of mass action that describe the reversible reactions rates and with $[Ca^{2+}]$ measurements as input.

The J_{Rec} is calculated by the sum of the fluxes produced by the SERCA, the sarcolemmal NCX and the mitochondria (MCU and NCE), which are described with Eqs. 57-60. As in the description of the buffers, it is assumed that these flows are uniformly distributed in the cytoplasm.

3.3.2 Multi-compartment estimation

We implemented a method to reduce the normalized root mean square error (NRMSE) obtained when compared experimental and simulated $\Delta[Ca^{2+}]_{cyto}$. The following function was used to simulate the flux of release elicited by a single AP

$$f_{Rel}(t) = a + \sum_{i=1}^{N} b_i e^{-\left(\frac{t-c_i}{d_i}\right)^2}, \quad (61)$$

where a, b_i, c_i and d_i are coefficients initially adjusted to fit the J_{Rel} estimated with the single-compartment model for each fiber type. This expression was used since it properly fits to the estimated release rate of Ca^{2+} and allowed us to reproduce the kinetic parameters. N=6 is the minimum number of terms that we required to obtain similar kinetic parameters to the estimated release rate of Ca^{2+} with the single-compartment model mentioned in the table 1. The coefficients obtained were used as an initial guess.

The simulation was performed iteratively, and in each iteration the coefficients of f_{Rel} were adjusted to minimize the differences between

experimental and simulated $\Delta[Ca^{2+}]_{cyto}$. In each iteration the function FMINCON of MATLAB 2021a was used to find the coefficients that minimize this difference.

Table 1. Parameters used for the multi-compartment model simulations of Ca^{2+} transients in skeletal muscle fibers types I, IIA, IIX/D and IIB skeletal muscle fibers.

Parameter	Description	Value		Reference
		IIA, IIX and IIB	I	
General				
L	Half sarcomere length	1 µm	1 µm	(Bolaños et al., 2008; Calderón et al., 2009)
R	Radius of sarcomere	0.5-0.7 µm	0.5-0.7 µm	(Hirose et al., 1994b; Hodge et al., 1954)
m	Longitudinal subdivisions	10	10	(Marcucci et al., 2018)
n	Radial subdivisions	5	5	(Marcucci et al., 2018)
V_{tot}	Half-sarcomere volumen ($V_T=\pi R^2L$)	0.78 μm^3	0.78 μm^3	(Present study)
V_{SR}	Volume of SR	7.4%	4.2%	(Eisenberg, 2011b)
V_{MITO}	Volume of MITO	5.1%	10.4%	(Chen et al., 2001; Eisenberg, 2011b)
V_{cyto}	Volume of cytoplasmic water	87.5%	85.4%	(Present study)
D	Ca^{2+} diffusion coefficient	0.7 $\mu m^2 s^{-1}$	0.7 $\mu m^2 s^{-1}$	(Stephen M. Baylor & Hollingworth, 2007b)
J_L	Constant leak flux			(Present study)
T	Absolute temperature	296.15K	296.15K	(Present study)
Pump rate for SERCA				
V_{SERCA}	Maximum pump rate for $[Ca^{2+}]$	2 µM/ms	0.4-1 µM/ms	(Ferguson & Franzini-Armstrong, 1988; Leberer & Pette, 1986)
k_{SERCA}	SERCA half-maximum pump $[Ca^{2+}]$	0.44 µM	0.38 µM/ms	(Campbell et al., 1991; Lytton et al., 1992)
h	Hill coefficient	2.1	2.2	(Lytton et al., 1992)
NCE				
$k_{NCE,Ca^{2+}}$	Ca^{2+} binding constant of NCE	1.1 mM	1.1 mM	(Marcucci et al., 2018)

k_{NCE,Na^+}	Na^+ binding constant of NCE	8.3 mM	8.3 mM	(Dash & Beard, 2008a)
$\Delta\Psi_{m,mito}$	Delta of Mitochondrial inner potential	190 mV	190 mV	(Dash & Beard, 2008a)
f_{NCE}	Multiplication factor NCE	0.92	0.92	(Marcucci et al., 2018)
$[Na]_{cyto}$	Cytosolic sodium concentration	10 mM	10 mM	(Wüst et al., 2017)
$[Na]_{mito}$	Mitochondrial Na^+ concentration	5 mM	5 mM	(Wüst et al., 2017)
MCU				
V_{MCU}	Maximum flux rate MCU	24.5 µM s^{-1}	111.8 µM s^{-1}	(Stephen Hollingworth et al., 2012; Sembrowich et al., 1985)
h_{MCU}	MCU hill coefficient	2	3.5	(Sembrowich et al., 1985)
$K_{d,MCU}$	MCU half-maximum pump $[Ca^{2+}]$	1.2 µM	1.97 µM	(Sembrowich et al., 1985)
NCX				
$K_{Ca,NCE}$	Ca^{2+} binding constant of NCX	3 mM	3 mM	(Donoso & Hidalgo Tapia, 1989)
$K_{Na,NCE}$	Na^+binding constant of NCE	72 mM	72 mM	(Donoso & Hidalgo Tapia, 1989)
$\Delta\Psi_m$	Delta of sarcolemmal inner potential	80 mV	80 mV	(Sperelakis, 2012)
$[Na]_{cyto}$	Cytosolic sodium concentration	10 mM	10 mM	(Sperelakis, 2012)
$[Na^{2+}]_{extra}$	Extracellular $[Na^+]$	140 mM	140 mM	(Sperelakis, 2012)
$[Ca^{2+}]_{extra}$	Extracellular $[Ca^{2+}]$	1 mM	1 mM	(Sperelakis, 2012)
Bulk Concentrations and Ca^{2+} and Mg^{2+} reaction rates				
$[Ca^{2+}]_{R,cyto}$	Resting free Ca^{2+} in cytoplasm (Cyto)	106 nM	105 nM	(Williams et al., 1990)
$[Ca^{2+}]_{R,SR}$	Resting free Ca^{2+} in SR	1.01 mM	1.14 mM	(Fryer & Stephenson, 1996)
$[Mg^{2+}]_{R,cyto}$	Resting free Mg^{2+} in cytoplasm (Cyto)	0.78 mM	0.78 mM	(Westerblad & Allen, 1992)
$[Trop]_T$	Trop binding sites concentration	240 µM	240 µM	(S M Baylor et al., 1983; Ebashi et al., 1969)
$[PV]_T$	PV binding sites concentration	1260-1500 µM	155 µM	(Heizmann, 1984; Leberer & Pette, 1986)

k_+^{PV}	PV binding rate	$0.417x10^8$ $M^{-1}s^{-1}$	$0.417x10^8$ $M^{-1}s^{-1}$	(Stephen M. Baylor & Hollingworth, 2007b)
k_-^{PV}	PV unbinding rate	0.5 s^{-1}	0.5 s^{-1}	(Stephen M. Baylor & Hollingworth, 2007b)
$[ATP]_T$	ATP binding sites concentration	6.06 - 8 mM	3.66 - 5 mM	(Hintz et al. 1982; Kushmerick et al. 1992; Racay, Gregory, and Schwaller 2006)
$[CSQ]_T$	CSQ concentration	82.8 mM	82.8 mM	(Murphy et al., 2009)
k_+^{CSQ}	CSQ binding rate	$3{\cdot}10^{-3}\mu M^{-1}s^{-1}$	$3{\cdot}10^{-3}\mu M^{-1}s^{-1}$	(Westerblad & Allen, 1994)
k_-^{CSQ}	CSQ unbinding rate	3 s^{-1}	3 s^{-1}	(Westerblad & Allen, 1994)
h^{CSQ}	CSQ hill coefficient	3	3	(Fénelon et al., 2012)
$[Mg^{2+}]_T$	Mg^{2+} concentration	3300 µM	3300 µM	(Westerblad & Allen, 1994)
k_+^{Mg}	Mg^{2+} binding rate to PV	$1.2{\cdot}10^5 M^{-1}s^{-1}$	$1.2{\cdot}10^5 M^{-1}s^{-1}$	(Westerblad & Allen, 1994)
k_-^{Mg}	Mg^{2+} unbinding rate to PV	3.4 s^{-1}	3.4 s^{-1}	(Westerblad & Allen, 1994)

For type II fibers, in several cases, different simulated values are used for fiber type IIA, IIX/D and IIB in order to reliably evidence the differences among these fibers.

Chapter 4

Results

In this chapter we calculate the concentration of the biding sites in free and bound forms at equilibrium, these values are used as the initial concentrations. We estimated the kinetics of [Ca^{2+}] produced by each mechanism during single transients. Then we apply these simulations to analyze the importance of the different mechanisms in the whole ECC phenomenon.

4.1 Conversion of fluorescence signals to [Ca^{2+}]

The calibration curve was fitted with the Boltzmann's equation and we obtained from Eq. 53 that the [Ca^{2+}] is 721.07 µM (pCa=-3.14202) when $F=(F_{max}+F_{min})/2$ (Fig. 6). Assuming a $[D]_T$ of 229.1 µM we obtain a K_d of 1.5977 10^5 μM^2 (229.1 µM×721.07 µM). Also, assuming that K_d for Mg^{2+} ($K_{d,Mg}$) in situ is 22.88 times higher than in vitro, such was obtained with Ca^{2+}(1.77 10^5 μM^2/7.76 10^5 μM^2) then $K_{d,Mg}$ in situ would be 148.72 mM (6.5 mM×22.88).

By taking a maximum fluorescence of 6.3635 A.U., for fibers type IIB and IIX, 4.9929 A.U. for IIA and 4.0139 A.U. for I, as derived from papers previously published by our group, and a K_d of 1.5977 10^5 μM^2, a F_{min} of 0.1427 A.U. and F_{max} of 150.88 A.U., by using the Eq. 53 The peak [Ca^{2+}] for the continuum of fiber types was: IIB and IIX: 16.58 µM, IIA: 12.77 µM and I: 10.13 µM (Fig. 10A). For the tetanic Ca^{2+} transients, subsequent peaks were

also calculated (slow: 11.24, 12.95, 14.81 and 16.47 µM; fast: 12.13, 12.29, 12.24 and 11.96 µM) (Fig. 2B). (Fig. 10).

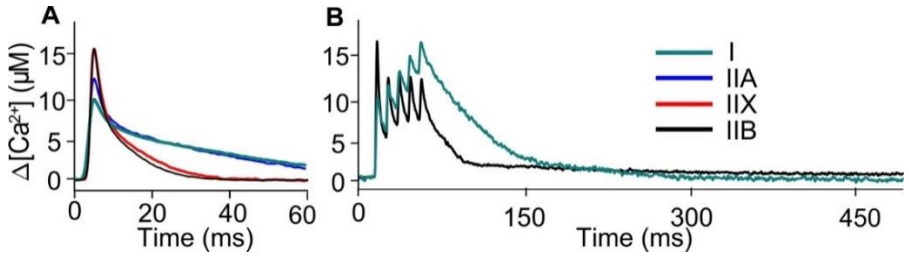

Fig. 10. Experimental measurements of $[Ca^{2+}]$ during Ca^{2+} transients elicited by a single and a train of APs. Fluorescence records generated with Mag-Fluo-4 AM are used to obtain the $\Delta[Ca^{2+}]$ in the cytoplasm produced by a single AP in fiber types I, IIA, IIX and IIB (A) and a train of 100 Hz and 5 APs in fibers slow and fast fibers (B).

The fluorescence signal of Mag-Fluo-4 is approximately 100 times greater when it is bound to Mg^{2+} and Ca^{2+} than when it is free (Invitrogen on-line), and the resting $[Mg^{2+}]$ and $[Ca^{2+}]$ are about 1 mM and 0.1 µM, respectively. Then, the fluorescence intensity at resting estate in the fiber (F_{rest}) is mainly produced by the indicator that is bound to Mg^{2+} and only a small fraction by Ca^{2+}. The fluorescence obtained for a $[Ca^{2+}]$ of 0.1 µM in the proposed model (Eq. 10) is 0.1914 A.U., which is associated with the fluorescence intensity produced by Ca^{2+}. The measured F_{rest} was 10.2 A.U., so the 1.87% ((0.1914 A.U.×100%)/10.2 A.U.) of the resting fluorescence is caused by Ca^{2+}.

4.2 Ca^{2+} movements produced during a twitch

4.2.1 Single-compartment estimation of release rate of Ca^{2+}

The release rate of Ca^{2+} was determined using measurements of single Ca^{2+} transients (Fig. 10) and by the sum of $d[Ca_T]/dt$ and J_{Rec}. The resulting release flux shows an increase with short duration and high magnitude produced by

the single AP, with differences in its shapes depending on the fiber type. However, differences between the experimental and the simulated $\Delta[Ca^{2+}]_{cyto}$ with the multi-compartment model are produced since the latter includes the Ca^{2+} diffusion, unlike the single-compartment model.

4.2.2 Multi-compartment estimation of release rate of Ca^{2+}

Table 2 shows the estimated kinetics parameters of f_{Rel} for the different fiber types. the release rate peak was higher for fast fibers (50% for IIA and 140% for IIB and IIX). The J_{Rel} estimated in tetanic Ca^{2+} transients shows that the last peak's amplitude is reduced over 15 times for slow fibers and over 7 times for fast fibers (Fig. 11. B; Table 2). Simulations with the multi-compartment model were performed to estimate Ca^{2+} movements in fibers types stimulated by a single AP. In all simulations, the f_{Rel} estimated was used as the input.

Fiber type	I	IIA	IIX	IIB
Peak amplitude (μM ms^{-1})	64.7	96.6	156.1	154.5
10-50% Rise time (ms)	1.8	1.3	1.2	1.4
10-90% Rise time (ms)	1.9	1.5	1.3	1.3
Half-width (ms)	2	1.7	1.4	1.3

Table 2. Kinetic parameters of release rate estimated after the coefficients adjustment.

4.2.3 Simulation of Ca^{2+} movements during Ca^{2+} transient

The $\Delta[Ca^{2+}]$ was estimated in three regions of the skeletal muscle fiber: the cytoplasm, the SR and the MITO (Fig. 11. A-C). There was a higher value in $\Delta[Ca^{2+}]_{MITO}$ for the slow fibers (up to seven times) as compared to the three fast fiber types. Regarding the SR compartment, our calculations show that the available Ca^{2+} is reduced up to ~70% (I:70%, IIA:81%, IIB and IIX:74%)

for single transients, but to almost 60% (I:62%, IIB:63%) after a train of five shocks.

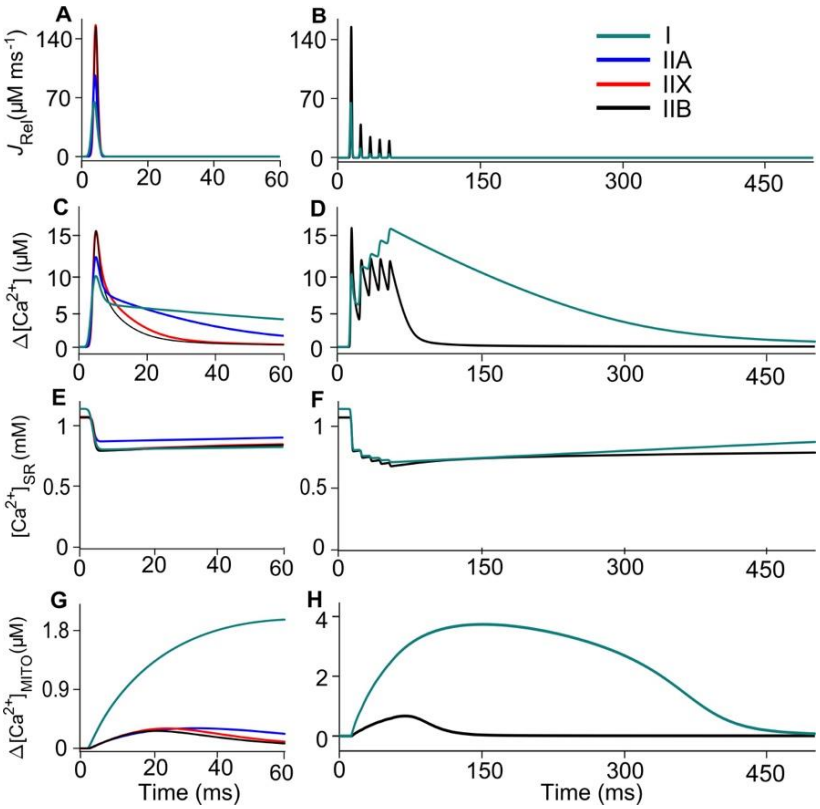

Fig. 11. Simulation of single Ca^{2+} transients in different fiber types. Release rate of Ca^{2+} estimated from the measurements of Δ[Ca^{2+}] in fibers type I, IIA, IIX and IIB (A and B). The model was used to reproduce the Δ[Ca^{2+}] obtained experimentally in the sarcoplasm (C and D) and to estimate the Δ[Ca^{2+}] in the SR (E and F) and MITO (G and H).

We also calculated the variations in [Ca^{2+}] for each buffer present in the three simulated compartments (Fig. 12 and 13), for both single (left column) and tetanic transients (right column). Fibers IIB and IIX form a close duple, in each case separated from the I and IIA duple. The total [Ca^{2+}] that remains in the cytoplasm [Ca^{2+}]$_T$ is the sum of the Δ[Ca^{2+}] in both free and bound forms

(Fig. 4I, J). Fibers IIB and IIX form a close duple, in each case separated from the I and IIA duple. Noticeably, the amount of Δ[CaDye] achieves only ~2% of the total Ca^{2+} available, thus ensuring unsaturation (I:1.3%, IIA:1.7%, IIB and IIX:2.2%).

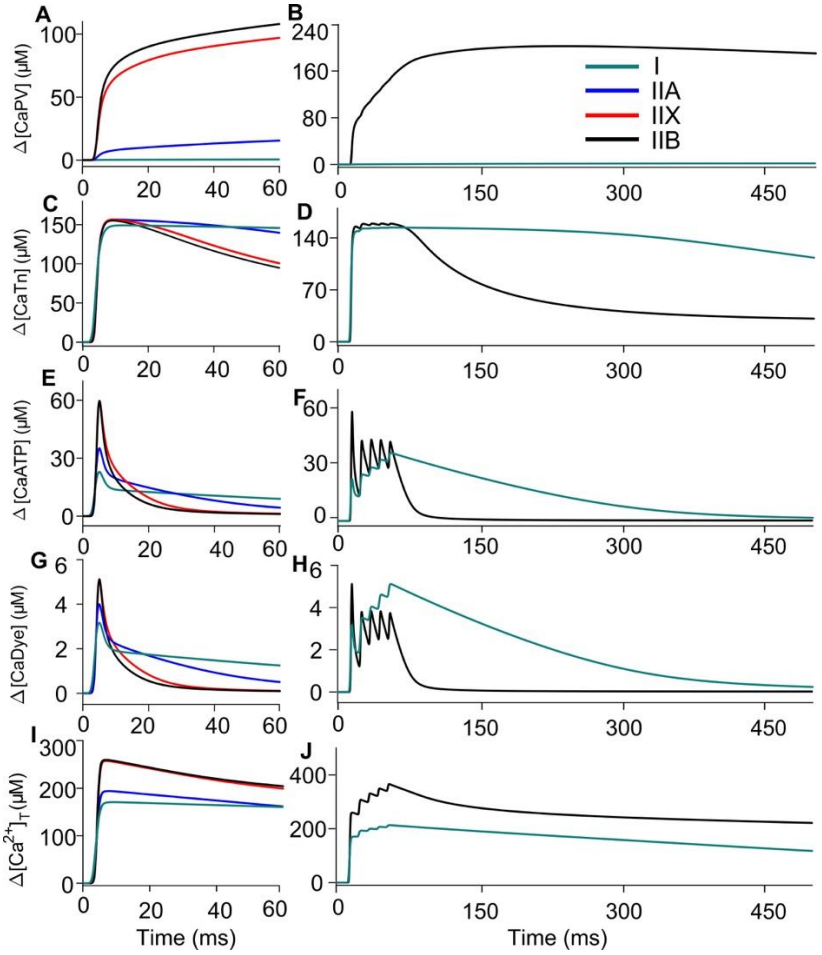

Fig. 12. Simulation of single (left column) and tetanic (right column) Ca^{2+} transients buffering in the sarcoplasm.. The Δ[Ca^{2+}] coupled to the sarcoplasmic buffers: PV (A and B), Tn (C and D), ATP (E and F) and the Dye (G and H). The total [Ca^{2+}] in the cytoplasm is calculated as the sum of the Δ[Ca^{2+}] in both free and bound forms (I and J).

Figure 13 shows the Ca^{2+} transients buffering in the SR and MITO (i.e., for CSQ and B, respectively). Since the concentration of Ca^{2+} in the SR decreases rapidly, is of relevance to notice the contribution of the Ca^{2+} unbinding from the CSQ molecules to inhibit a complete drop of [Ca^{2+}] inside the SR.

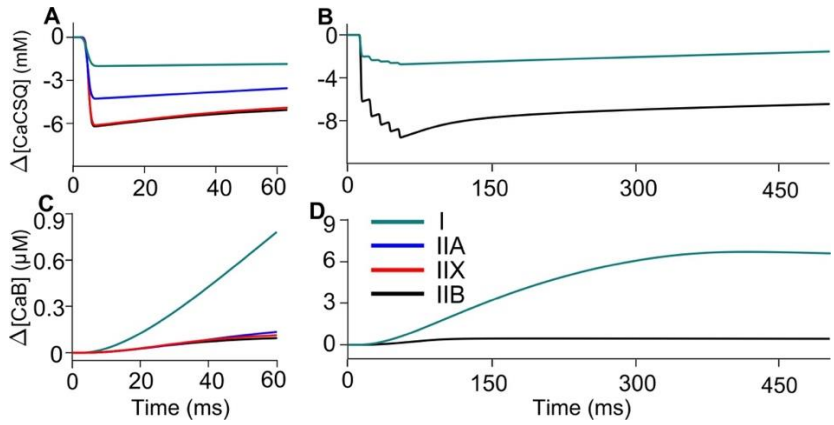

Fig. 13. Simulation of single (left column) and tetanic (right column) Ca^{2+} transients buffering in the SR and MITO. The CSQ (A and B), and the B (C and D) kinetics are shown.

We found that during the tetanic stimulation, the SERCA (Fig. 6A, B), in IIB fibers achieved 0.95, of its maximum capacity 0.6 ms after the first release rate peak and in fiber type I 0.94 after 0.3 ms. Indicating the SERCA mechanism achieves almost its saturation in a short time compared with the other mechanisms. Interestingly, the maximum Ca^{2+} extruded from the cytoplasm by the NCX was 2-3-fold higher in fibers type IIA, IIX and IIB, respectively, than in type I (Fig. 6C). This behavior was also observed for a train of transients (Fig. 6D). However, the [Ca^{2+}] returned into the cytoplasm by the SOCE even after 5 shocks was found too low compared to the average [Ca^{2+}] in the cytoplasm and the SR, being 27.59 nM and 186.72 nM in slow and fast (Fig. 6E, F).

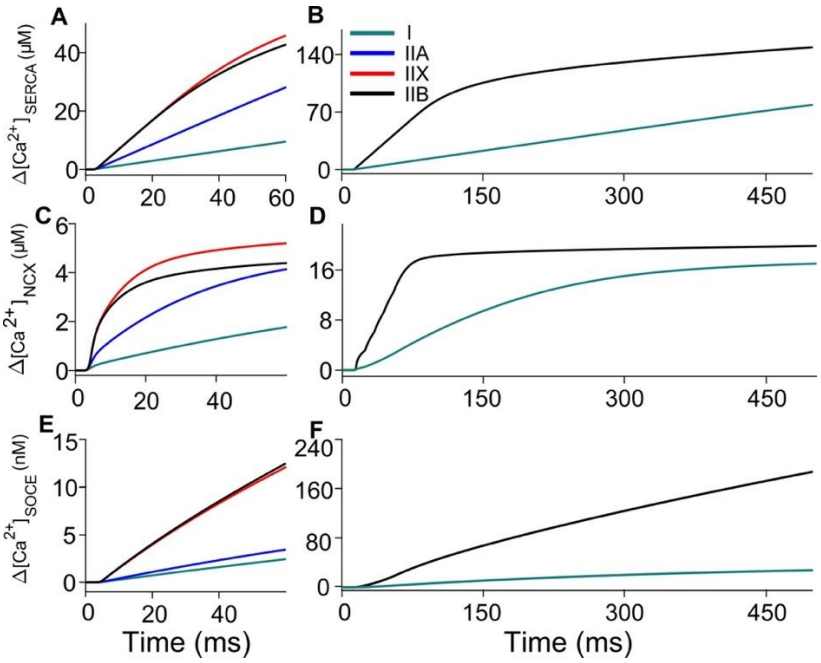

Fig. 13. Simulation of single (left column) and tetanic (right column) Ca^{2+} transients fluxes across the sarcolemma in the continuum of fiber types. The $[Ca^{2+}]$ is recaptured from the cytoplasm by the SERCA (A and B), extruded to the extracellular space through the NCX (C and D) and entered to the sarcoplasm through the SOCE (E and F). The fluxes were spatially averaged across the sarcoplasm.

Fiber type	I	IIA	IIX	IIB	I	IIB
	Single				Tetanic	
Maximum value						
$\Delta[CaTn]_{max}$ (μM)	149.09	156.5	156.56	155.12	154	159.19
$\Delta[CaPv]_{max}$ (μM)	0.54	15.51	97.02	108.02	1.74	202.48
$\Delta[CaATP]_{max}$ (μM)	22.89	35.12	59.52	59.65	37.17	59.64
$\Delta[CaDye]_{max}$ (μM)	3.16	3.99	5.1	5.12	5.12	5.12
$\Delta[CaB]_{max}$ (μM)	0.78	0.13	0.11	0.09	6.67	0.45
$\Delta[Ca^{2+}]_{NCX,max}$ (μM)	1.77	4.14	5.19	4.39	17.03	19.86
$\Delta[Ca^{2+}]_{SERCA,max}$ (μM)	9.51	28.1	45.86	42.73	78.56	148.68
$\Delta[Ca^{2+}]_{SOCE,max}$ (nM)	2.44	3.45	12.13	12.52	27.59	186.72
$\Delta[Ca^{2+}]_{MITO,max}$ (μM)	1.97	0.31	0.3	0.26	3.73	0.67
$\Delta[Ca^{2+}]_{T,max}$ (μM)	170.83	194.06	257.54	259.58	213.26	365.81

$\|\Delta[CaCSQ]\|_{max}$ (mM)	2.01	4.28	6.13	6.2	2.75	9.57
$\|\Delta[Ca^{2+}]_{SR}\|_{max}$ (mM)	0.34	0.2	0.27	0.28	0.44	0.4
Area under the curve						
$\Delta[CaTn]_{AUC}$ (µM ms)	8216.3	8346.67	7335.07	7044.91	69174.52	32797.71
$\Delta[CaPv]_{AUC}$ (µM ms)	21.43	650.09	4618.92	5199.67	606.23	91283.22
$\Delta[CaATP]_{AUC}$ (µM ms)	674.78	678.67	529.44	433.31	6982.42	2214.72
$\Delta[CaDye]_{AUC}$ (µM ms)	93.84	77.83	45.9	37.57	966.65	191.91
$\Delta[CaB]_{AUC}$ (µM ms)	18.17	3.47	3.28	2.89	2219.78	189.72
$\Delta[Ca^{2+}]_{NCX,AUC}$ (µM ms)	57.71	155.59	239.91	206.94	5831.1	8747.61
$\Delta[Ca^{2+}]_{SERCA,AUC}$ (µM ms)	275.01	810.13	1472.5	1410.69	19506.55	54574.14
$\Delta[Ca^{2+}]_{SOCE,AUC}$ (nM ms)	69.84	101.09	361.32	370.87	7902.54	50173.87
$\Delta[Ca^{2+}]_{MITO,AUC}$ (µM ms)	82.34	13.88	11.57	9.72	1087.27	50.42
$\Delta[Ca^{2+}]_{T,AUC}$ (µM ms)	9304.1	10000.33	12675.45	12835.06	80815.67	127098.86
$\|\Delta[CaCSQ]\|_{AUC}$ (mM ms)	108.73	219.44	304.72	310.34	1045.85	3550.85
$\|\Delta[Ca^{2+}]_{SR}\|_{AUC}$ (mM ms)	18.36	10.33	13.86	14.08	172.86	155.07

Table 3. Maximum values reached and area under the curve during the simulated time interval for a single and tetanic Ca^{2+} transient in muscle fibers.

4.2.4 Influence of reuptake mechanisms on the decay phase of the single Ca^{2+} transients

The decay phase of the Ca^{2+} transient can be fitted with a biexponential function (with τ_1 and τ_2). An increase of 50% in the PV content differentially changed the τ_1 of the IIB-IIX group by -6.0% and of the IIA-I group by 16.2%, whilst the τ_2 always decreased, by 26.1% in the IIB-IIX group and 6.1% in the IIA-I group (Fig. 14).

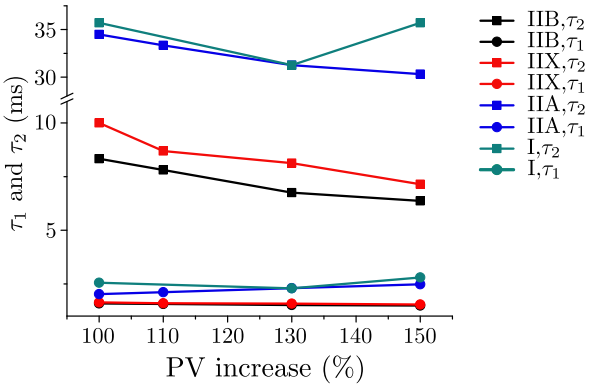

Fig. 14. The simulations were performed with different values of [PV] and the decay phase is fitted with a biexponential function. The changes in cytoplasmic $\Delta[Ca^{2+}]$ decay phase was estimated with the parameters τ_1 and τ_2 of the biexponential function.

Chapter 5

Discussion

5.1 Discussion

The main findings of the present work were: *i)* during a single twitch, the sarcoplasmic peak [Ca^{2+}] for fibers type IIB and IIX is between 15-25 µM, and for fibers type I and IIA reaches 6-12 µM, *ii)* both the pattern of change and the peak concentrations of the Ca^{2+}-bound species in the sarcomere, the sarcolemma and inside the SR showed the order IIB≥IIX>IIA>I, *iii)* the mitochondrial peak [Ca^{2+}] and the MITO buffers saturation showed the pattern I>>IIA>>IIX≥IIB.

Previous models of mammalian ECC were affected by either uncertainty in the classification of fiber types, unreliable kinetics of the raw Ca^{2+} signals due to the use of slow Ca^{2+} dyes or the lack of information about the role of several intracellular compartments in Ca^{2+} handling. To overcome these limitations, we based our model on the first calibration of Ca^{2+} transients of the four main fiber types found in mammals, obtained using the fast Ca^{2+} dye Mag-Fluo-4, and integrated new information gathered on MITO, SR, NCX and SOCE, along basic knowledge on sarcoplasmic Ca^{2+} movements and buffering.

5.1.1 Reliable [Ca^{2+}] kinetics: slow vs fast Ca^{2+} dyes

The Ca^{2+} transients modeled in the present study were obtained with the fast Ca^{2+} dye Mag-Fluo-4. Two issues with quantitative impact on the results deserve attention: the biochemical properties of the dye and its loading conditions.

This dye has a 2:1 Mag-Fluo-4—Ca^{2+} binding stoichiometry, with an *in situ* K_d of $1.652x10^5$ μM^2 (Milán et al., 2021). This explains why it can reliably track the Ca^{2+} transients even in the fastest types, i.e., IIB, demonstrate subtle differences among all four fiber types and resolve every peak in a tetanic transient, being a trustable source for the model. On the other side, since the fibers typically have ~200 µM of Mag-Fluo-4 (Milán et al., 2021), we found that less than ~3% of the dye is bound to Ca^{2+}.

The very low affinity of the dye, and the lack of saturation, confer Mag-Fluo-4 the ability to determine a trustable peak sarcoplasmic [Ca^{2+}]. Our results with Mag-Fluo-4 (present study and (Milán et al., 2021)) join those with Mag-Fura-2 (Baylor and Hollingworth, 2003, 2007) showing that the peak [Ca^{2+}] in fast fibers IIX or IIB is typically between 15 and 25 µM in mammalian skeletal muscle (16-22°C). The numbers for type I and IIA fibers also agree with a study reporting peak Ca^{2+} for soleus slow fibers (Hollingworth et al., 2012). That work, however, may have really used type I and IIA fibers, because the periphery of the soleus muscles of mouse used in the experiments have both types of fibers evenly distributed, as we have verified using specific antibodies and confocal microscopy (not shown). In conclusion, that paper and our results agree in that peak [Ca^{2+}] for fibers types I and IIA is between 6 and 12 µM (Hollingworth et al., 2012). The above numbers are one order of magnitude higher than those misleadingly reported with slow, saturable dyes (Olsson et al., 2020; Weiss et al., 2010; Koenig et al., 2019; Marcucci et al., 2018). This fact may, for instance, reduce the estimated maximum rate of

Ca^{2+} flux during SOCE or ECCE activations (Launikonis et al., 2009; Koenig et al., 2019), since this value depends on the driving force for Ca^{2+} (Launikonis et al., 2010), which in turn is reduced if sarcoplasmic [Ca^{2+}] is raised. Trustable peak sarcoplasmic [Ca^{2+}] also permits a better quantitation of the chemical species involved in ECC ([CaTn], [CaTNS], [CaPV], [CaATP], [CaDye], free [Ca^{2+}], etc), including peak [Ca^{2+}] inside compartments such as MITO.

5.1.2 The Ca^{2+} release

Differences between the release rate of Ca^{2+} obtained with the single-compartment analysis and the coefficients adjustment with the multi-compartment model were found. Those differences are presumably because the single-compartment analysis does not consider the Ca^{2+} diffusion within the sarcomere. The coefficients adjustment increases the computational complexity of the simulation, but permits to consider valuable information, that is, the geometry of the sarcomere and the diffusion coefficient of Ca^{2+} to finally determine the release rate of Ca^{2+}.

A function chosen empirically (Eq. 61) permitted to simulate the release rate of Ca^{2+}. Although other functions have also been proposed (S M Baylor & Hollingworth, 1998; Cannell & Allen, 1984; Gillis et al., 1982), we could not reproduce all the kinetic parameters obtained for the release rate of Ca^{2+}. In Baylor *et al.* (2007) and Hollingworth et al. (2012) the coefficients of the chosen function were adjusted to reproduce the full-duration at half-maximum (FDHM) of 1.7 ms and 1.6 ms for slow and fast fibers, respectively, obtained with a single-compartment analysis using Mag-Fura-2 signals in mouse fibers (S M Baylor & Hollingworth, 2003b). In our

simulations, the coefficients were successfully adjusted to reproduce the Ca^{2+} kinetic obtained in different fiber types using Mag-Fluo-4 AM signals.

The simulation of Ca^{2+} movements indicate that the release rate of Ca^{2+} elicited by a single AP has differences in its kinetic parameters according to the fiber type. The peak flux differences are consistent with measurements of RyR content in fast fibers, which are about 3 times higher than the slow ones; whilst type IIA are intermediate between I and IIB (Appelt et al., 1989; Damiani & Margreth, 1994; Franzini-Armstrong et al., 1988; S Hollingworth & Marshall, 1981; Lamb & Walsh, 1987; Renganathan et al., 1998). The similarities between half-width, rise time and decay time in different fiber types can be explained by the fact that all fiber types share the RyR1 isoform, which is in part responsible for the release rate of Ca^{2+} (Lee et al., 1991).

Importantly, the model demonstrates that the conditions of loading of the Mag-Fluo-4 in our experiments lead to a [Dye] that is far from saturation. It was unknown if the saturation may have affected previous data published using Mag-Fluo-4 (Calderón et al., 2010, 2014b). Since our cells typically have around 200 µM of Mag-Fluo-4, and the model showed that during the twitch the [Ca^{2+}-Dye] is about 15 µM, only ~7% of the dye is bound to Ca^{2+}. This suggests that previous published data is not affected by this artifact, and that the [Dye] used in the experiments can be reduced. Furthermore, this rises a new advantage of Mag-Fluo over other dyes such as Fura-2 or Fluo-4, which become saturated inside the skeletal muscle fibers.

5.1.3 The mechanisms of Ca^{2+} reuptake

The peak amplitude of [Ca^{2+}] recaptured reached by the MITO and NCX mechanisms are much smaller than $\Delta[Ca^{2+}]$ in the cytoplasm. However, due

the differences in the mitochondrial volume between fiber types, the [Ca^{2+}] in the MITO is higher in fibers I and IIA than in IIX and IIB.

Our simulations were based on measurements of [Ca^{2+}] in the cytoplasm of different fiber types. However, experimental measurements of [Ca^{2+}] in the SR and MITO, differentiating the kinetics of fiber types I, IIA, IIX and IIB, are still required to validate the simulated results in these compartments.

5.1.4 The classification of fiber types

Preceding models addressed ECC in one or two fiber types, mainly because most previous functional and biochemical information came from a dichotomic approach of muscle fibers: either slow vs fast, or type I vs type II (Bakker et al., 2017; S M Baylor & Hollingworth, 2003a; Stephen M. Baylor & Hollingworth, 2007a; Gillis et al., 1982; Stephen Hollingworth et al., 2012; Marcucci et al., 2018). Also, simulations that have recently become spatially and mathematically more complex, have remained biochemically oversimplified (Holash & MacIntosh, 2019; M. Wang et al., 2020). By taking as experimental source Ca^{2+} transients obtained in molecularly typed fibers covering the whole spectra from I to IIB, our model goes beyond the dichotomic approach.

The fact that molecular and biochemical differences (i.e. isoforms and their biochemical properties) underlie the differences in ECC among fiber types has been described in detail elsewhere and we refer the readers to those papers (Bottinelli & Reggiani, 2000; Calderón et al., 2010, 2011, 2014a). However, there is still a lack of molecular and biochemical information particularly for fibers type IIA and IIX. Our adjustments and results for these two types of fibers seem reliable because most values obtained laid between those of fibers type I and IIB. This agrees with the fact that fibers IIA and IIX showed

kinetics of the Ca^{2+} transients, Ca^{2+} sensitivity and other dynamic properties, which are mostly intermediate between I and IIB (Calderón et al., 2010). Together, this confirms that most values of molecular, biochemical and physiological parameters follow a continuum from I, to IIA, to IIX, to IIB.

5.1.5 Final remarks

Although the above analyses give averages of peak sarcoplasmic/compartments [Ca^{2+}], spatially refined models for fast fibers have shown up to a 20-fold gradient in the sarcoplasmic [Ca^{2+}], depending on the distance of a subcellular region from the Ca^{2+} release units (Baylor and Hollingworth, 2007; Holash and MacIntosh, 2019; Hollingworth et al., 2012).This phenomenon is also expected to apply to all fiber types, but the magnitude of those gradients inside the fibers was not explored in the present study.

Also, since our Ca^{2+}-bound chemical species had higher concentrations than those recently estimated, the thermal changes associated with ECC in mammalian muscle should be higher than proposed (Barclay and Launikonis, 2021). Our model may be a source to build a more complete model on thermal changes in all fiber types during single and tetanic stimulation.

5.2 Conclusion

Our mathematical, comprehensive model allows us to gain insight into the kinetics of the Ca^{2+} transients obtained with the fast Ca^{2+} dye Mag-Fluo-4, for the continuum of skeletal muscle fiber types. Sarcoplasmic peak [Ca^{2+}] is one order of magnitude higher than reported with slow dyes. The magnitudes of change of the Ca^{2+}-bound forms of the Ca^{2+} buffers studied follow the order IIB≥IIX>IIA>I, except for mitochondrial peak [Ca^{2+}] which showed the pattern I>>IIA>>IIX≥IIB. The kinetics for fibers IIA and IIX proved to be

intermediate between I and IIB fibers, supporting dynamic data. The results may help better quantitate SOCE fluxes and thermal changes in mammalian fiber types in the future and support the use of fast Ca^{2+} dyes for most experimental approaches in skeletal muscle.

References

Appelt, D., Buenviaje, B., Champ, C., & Franzini-Armstrong, C. (1989). Quantitation of “junctional feet” content in two types of muscle fiber from hind limb muscles of the rat. *Tissue & Cell*, *21*(5), 783–794. http://www.ncbi.nlm.nih.gov/pubmed/2617518

Bakker, A. J., Cully, T. R., Wingate, C. D., Barclay, C. J., & Launikonis, B. S. (2017). Doublet stimulation increases Ca2+ binding to troponin C to ensure rapid force development in skeletal muscle. *Journal of General Physiology*, *149*(3), 323–334. https://doi.org/10.1085/jgp.201611727

Balnave, C. D., & Allen, D. G. (1998). Evidence for Na^{+} /Ca^{2+} exchange in intact single skeletal muscle fibers from the mouse. *American Journal of Physiology-Cell Physiology*, *274*(4), C940–C946. https://doi.org/10.1152/ajpcell.1998.274.4.C940

Baylor, S M, Chandler, W. K., & Marshall, M. W. (1983). Sarcoplasmic reticulum calcium release in frog skeletal muscle fibres estimated from Arsenazo III calcium transients. *The Journal of Physiology*, *344*, 625–666. http://www.ncbi.nlm.nih.gov/pubmed/6655593

Baylor, S M, & Hollingworth, S. (1998). Model of sarcomeric Ca2+ movements, including ATP Ca2+ binding and diffusion, during activation of frog skeletal muscle. *The Journal of General Physiology*, *112*(3), 297–316. http://www.ncbi.nlm.nih.gov/pubmed/9725890

Baylor, S M, & Hollingworth, S. (2003a). Sarcoplasmic reticulum calcium release compared in slow-twitch and fast-twitch fibres of mouse muscle. *The Journal of Physiology*, *551*(1), 125–138. https://doi.org/10.1113/jphysiol.2003.041608

Baylor, S M, & Hollingworth, S. (2003b). Sarcoplasmic reticulum calcium release compared in slow-twitch and fast-twitch fibres of mouse muscle. *The Journal of Physiology*, *551*(Pt 1), 125–138. https://doi.org/10.1113/jphysiol.2003.041608

Baylor, Stephen M., & Hollingworth, S. (2007a). Simulation of Ca2+

movements within the sarcomere of fast-twitch mouse fibers stimulated by action potentials. *The Journal of General Physiology*, *130*(3), 283–302. https://doi.org/10.1085/jgp.200709827

Baylor, Stephen M., & Hollingworth, S. (2007b). Simulation of Ca2+ Movements within the Sarcomere of Fast-Twitch Mouse Fibers Stimulated by Action Potentials. *The Journal of General Physiology*, *130*(3), 283–302. https://doi.org/10.1085/jgp.200709827

Baylor, Stephen M., & Hollingworth, S. (2011). Calcium indicators and calcium signalling in skeletal muscle fibres during excitation–contraction coupling. *Progress in Biophysics and Molecular Biology*, *105*(3), 162–179. https://doi.org/10.1016/j.pbiomolbio.2010.06.001

Baylor, Stephen M, & Hollingworth, S. (2012). Intracellular calcium movements during excitation-contraction coupling in mammalian slow-twitch and fast-twitch muscle fibers. *The Journal of General Physiology*, *139*(4), 261–272. https://doi.org/10.1085/jgp.201210773

Berchtold, M. W., Brinkmeier, H., & Müntener, M. (2000). Calcium ion in skeletal muscle: Its crucial role for muscle function, plasticity, and disease. In *Physiological Reviews* (Vol. 80, Issue 3, pp. 1215–1265). American Physiological Society. https://doi.org/10.1152/physrev.2000.80.3.1215

Bolaños, P., Guillen, A., Rojas, H., Boncompagni, S., & Caputo, C. (2008). The use of CalciumOrange-5N as a specific marker of mitochondrial Ca2+ in mouse skeletal muscle fibers. *Pflügers Archiv - European Journal of Physiology*, *455*(4), 721–731. https://doi.org/10.1007/s00424-007-0312-5

Bottinelli, R., & Reggiani, C. (2000). Human skeletal muscle fibres: molecular and functional diversity. *Progress in Biophysics and Molecular Biology*, *73*(2–4), 195–262. http://www.ncbi.nlm.nih.gov/pubmed/10958931

Calderón, J. C., Bolaños, P., & Caputo, C. (2010). Myosin heavy chain isoform composition and Ca $^{2+}$ transients in fibres from enzymatically dissociated murine soleus and extensor digitorum longus muscles. *The Journal of Physiology*, *588*(1), 267–279. https://doi.org/10.1113/jphysiol.2009.180893

Calderón, J. C., Bolaños, P., & Caputo, C. (2011). Kinetic changes in tetanic Ca 2+ transients in enzymatically dissociated muscle fibres under repetitive stimulation. *Journal of Physiology*, *589*(21), 5269–5283. https://doi.org/10.1113/jphysiol.2011.213314

Calderón, J. C., Bolaños, P., & Caputo, C. (2014a). The excitation–contraction coupling mechanism in skeletal muscle. *Biophysical Reviews*, *6*(1), 133–160. https://doi.org/10.1007/s12551-013-0135-x

Calderón, J. C., Bolaños, P., & Caputo, C. (2014b). Tetanic Ca2+ transient differences between slow- and fast-twitch mouse skeletal muscle fibres: a comprehensive experimental approach. *Journal of Muscle Research and Cell Motility*, *35*(5–6), 279–293. https://doi.org/10.1007/s10974-014-9388-7

Calderón, J. C., Bolaños, P., Torres, S. H., Rodríguez-Arroyo, G., & Caputo, C. (2009). Different fibre populations distinguished by their calcium transient characteristics in enzymatically dissociated murine flexor digitorum brevis and soleus muscles. *Journal of Muscle Research and Cell Motility*, *30*(3–4), 125–137. https://doi.org/10.1007/s10974-009-9181-1

Campbell, A. M., Kessler, P. D., Sagara, Y., Inesi, G., & Fambrough, D. M. (1991). Nucleotide sequences of avian cardiac and brain SR/ER Ca(2+)-ATPases and functional comparisons with fast twitch Ca(2+)-ATPase. Calcium affinities and inhibitor effects. *The Journal of Biological Chemistry*, *266*(24), 16050–16055. http://www.ncbi.nlm.nih.gov/pubmed/1831452

Cannell, M. B., & Allen, D. G. (1984). Model of calcium movements during activation in the sarcomere of frog skeletal muscle. *Biophysical Journal*. https://doi.org/10.1016/S0006-3495(84)84238-1

Caputo, C., & Bolaños, P. (1994). Fluo-3 signals associated with potassium contractures in single amphibian muscle fibres. *Journal of Physiology*. https://doi.org/10.1113/jphysiol.1994.sp020423

Caputo, C., Edman, K. A., Lou, F., & Sun, Y. B. (1994). Variation in myoplasmic Ca2+ concentration during contraction and relaxation studied by the indicator fluo-3 in frog muscle fibres. *The Journal of Physiology*. https://doi.org/10.1113/jphysiol.1994.sp020237

Chen, G., Carroll, S., Racay, P., Dick, J., Pette, D., Traub, I., Vrbova, G., Eggli, P., Celio, M., & Schwaller, B. (2001). Deficiency in parvalbumin increases fatigue resistance in fast-twitch muscle and upregulates mitochondria. *American Journal of Physiology-Cell Physiology*, *281*(1), C114–C122. https://doi.org/10.1152/ajpcell.2001.281.1.C114

Damiani, E., & Margreth, A. (1994). Characterization study of the ryanodine receptor and of calsequestrin isoforms of mammalian skeletal muscles in relation to fibre types. *Journal of Muscle Research and Cell Motility*,

15(2), 86–101. https://doi.org/10.1007/BF00130421

Dash, R. K., & Beard, D. A. (2008a). Analysis of cardiac mitochondrial Na+-Ca2+ exchanger kinetics with a biophysical model of mitochondrial Ca2+ handling suggests a 3:1 stoichiometry. *The Journal of Physiology*, *586*(13), 3267–3285. https://doi.org/10.1113/jphysiol.2008.151977

Dash, R. K., & Beard, D. A. (2008b). Analysis of cardiac mitochondrial Na + -Ca 2+ exchanger kinetics with a biophysical model of mitochondrial Ca 2+ handing suggests a 3: 1 stoichiometry. *The Journal of Physiology*, *586*(13), 3267–3285. https://doi.org/10.1113/jphysiol.2008.151977

Delbono, O., & Stefani, E. (1993). Calcium transients in single mammalian skeletal muscle fibres. *The Journal of Physiology*, *463*, 689–707. http://www.ncbi.nlm.nih.gov/pubmed/8246201

Donaldson, S. K., Best, P. M., & Kerrick, G. L. (1978). Characterization of the effects of Mg2+ on Ca2+- and Sr2+-activated tension generation of skinned rat cardiac fibers. *The Journal of General Physiology*, *71*(6), 645–655. https://doi.org/10.1085/jgp.71.6.645

Donoso, P., & Hidalgo Tapia, M. C. (1989). Sodium-calcium exchange in transverse tubules isolated from frog skeletal muscle. *BBA - Biomembranes*. http://repositorio.uchile.cl/handle/2250/160754

Dubowitz, V., & Pearse, A. G. E. (1960). A comparative histochemical study of oxidative enzyme and phosphorylase activity in skeletal muscle. *Histochemie*, *2*(2), 105–117. https://doi.org/10.1007/BF00744575

Ebashi, S., Endo, M., & Otsuki, I. (1969). Control of muscle contraction. *Quarterly Reviews of Biophysics*, *2*(4), 351–384. http://www.ncbi.nlm.nih.gov/pubmed/4935801

Eisenberg, B. R. (2011a). Quantitative Ultrastructure of Mammalian Skeletal Muscle. In *Comprehensive Physiology* (pp. 73–112). John Wiley & Sons, Inc. https://doi.org/10.1002/cphy.cp100103

Eisenberg, B. R. (2011b). Quantitative Ultrastructure of Mammalian Skeletal Muscle. In *Comprehensive Physiology* (pp. 73–112). John Wiley & Sons, Inc. https://doi.org/10.1002/cphy.cp100103

Engel, W. K. (1998). The essentially of histo- and cytochemical studies muscle in the investigation of neuromuscular disease. In *Neurology* (Vol. 51, Issue 3, p. 655). Wolters Kluwer Health, Inc. on behalf of the American Academy of Neurology. https://doi.org/10.1212/wnl.51.3.778

Fall, C. P. (2004). Computational Cell Biology. In *Computational Cell*

Biology. Springer New York. https://doi.org/10.1007/b97701

Fénelon, K., Lamboley, C. R. H., Carrier, N., & Pape, P. C. (2012). Calcium buffering properties of sarcoplasmic reticulum and calcium-induced Ca(2+) release during the quasi-steady level of release in twitch fibers from frog skeletal muscle. *The Journal of General Physiology*, *140*(4), 403–419. https://doi.org/10.1085/jgp.201110730

Ferguson, D. G., & Franzini-Armstrong, C. (1988). The Ca2+ ATPase content of slow and fast twitch fibers of guinea pig. *Muscle & Nerve*, *11*(6), 561–570. https://doi.org/10.1002/mus.880110607

Franzini-Armstrong, C., Ferguson, D. G., & Champ, C. (1988). Discrimination between fast- and slow-twitch fibres of guinea pig skeletal muscle using the relative surface density of junctional transverse tubule membrane. *Journal of Muscle Research & Cell Motility*, *9*(5), 403–414. https://doi.org/10.1007/BF01774067

Fraysse, B., Rouaud, T., Millour, M., Fontaine-Pérus, J., Gardahaut, M.-F., & Levitsky, D. O. (2001). Expression of the Na^{+}/Ca^{2+} exchanger in skeletal muscle. *American Journal of Physiology-Cell Physiology*, *280*(1), C146–C154. https://doi.org/10.1152/ajpcell.2001.280.1.C146

Fryer, M. W., & Stephenson, D. G. (1996). Total and sarcoplasmic reticulum calcium contents of skinned fibres from rat skeletal muscle. *The Journal of Physiology*, *493 (Pt 2*, 357–370. http://www.ncbi.nlm.nih.gov/pubmed/8782101

Füchtbauer, E. M., Rowlerson, A. M., Götz, K., Friedrich, G., Mabuchi, K., Gergely, J., & Jockusch, H. (1991). Direct correlation of parvalbumin levels with myosin isoforms and succinate dehydrogenase activity on frozen sections of rodent muscle. *Journal of Histochemistry & Cytochemistry*, *39*(3), 355–361. https://doi.org/10.1177/39.3.1825216

Gillis, J. M., Thomason, D., Lefèvre, J., & Kretsinger, R. H. (1982). Parvalbumins and muscle relaxation: a computer simulation study. *Journal of Muscle Research and Cell Motility*, *3*(4), 377–398. http://www.ncbi.nlm.nih.gov/pubmed/7183710

Grynkiewicz, G., Poenie, M., & Tsien, R. Y. (1985). A new generation of Ca2+ indicators with greatly improved fluorescence properties. *The Journal of Biological Chemistry*, *260*(6), 3440–3450. http://www.ncbi.nlm.nih.gov/pubmed/3838314

Heizmann, C. W. (1984). Parvalbumin, and intracellular calcium-binding protein; distribution, properties and possible roles in mammalian cells.

Experientia, *40*(9), 910–921. https://doi.org/10.1007/BF01946439

Heizmann, C. W., Berchtold, M. W., & Rowlerson, A. M. (1982). Correlation of parvalbumin concentration with relaxation speed in mammalian muscles. *Proceedings of the National Academy of Sciences of the United States of America*, *79*(23), 7243–7247. https://doi.org/10.1073/PNAS.79.23.7243

Helms, V. (2018). *Principles of Computational Cell Biology : From Protein Complexes to Cellular Networks.* John Wiley & Sons, Incorporated.

Hidalgo, C., González, M. E., & García, A. M. (1986). Calcium transport in transverse tubules isolated from rabbit skeletal muscle. *Biochimica et Biophysica Acta*, *854*(2), 279–286. http://www.ncbi.nlm.nih.gov/pubmed/3080021

Hill, J. A., & Olson, E. N. (2012). Muscle. In *Muscle* (Vols. 1–2). Elsevier Inc. https://doi.org/10.1016/C2009-0-61900-0

Hintz, C. S., Chi, M. M., Fell, R. D., Ivy, J. L., Kaiser, K. K., Lowry, C. V., & Lowry, O. H. (1982). Metabolite changes in individual rat muscle fibers during stimulation. *American Journal of Physiology-Cell Physiology*, *242*(3), C218–C228. https://doi.org/10.1152/ajpcell.1982.242.3.C218

Hirose, K., Franzini-Armstrong, C., Goldman, Y. E., & Murray, J. M. (1994a). Structural changes in muscle crossbridges accompanying force generation. *The Journal of Cell Biology*, *127*(3), 763–778. https://doi.org/10.1083/JCB.127.3.763

Hirose, K., Franzini-Armstrong, C., Goldman, Y. E., & Murray, J. M. (1994b). Structural changes in muscle crossbridges accompanying force generation. *The Journal of Cell Biology*, *127*(3), 763–778. https://doi.org/10.1083/JCB.127.3.763

Hirota, A., Knox Chandler, W., Southwick, P. L., & Waggoner, A. S. (1989). Calcium signals recorded from two new purpurate indicators inside frog cut twitch fibers. *Journal of General Physiology*, *94*(4), 597–631. https://doi.org/10.1085/jgp.94.4.597

Hodge, A. J., Huxley, H. E., & Spiro, D. (1954). Electron microscope studies on ultrathin sections of muscle. *The Journal of Experimental Medicine*, *99*(2), 201–206. https://doi.org/10.1084/JEM.99.2.201

Holash, R. J., & MacIntosh, B. R. (2019). A stochastic simulation of skeletal muscle calcium transients in a structurally realistic sarcomere model using MCell. *PLOS Computational Biology*, *15*(3), e1006712.

https://doi.org/10.1371/journal.pcbi.1006712

Hollingworth, S, & Marshall, M. W. (1981). A comparative study of charge movement in rat and frog skeletal muscle fibres. *The Journal of Physiology*, *321*(1), 583–602. https://doi.org/10.1113/jphysiol.1981.sp014004

Hollingworth, Stephen, Kim, M. M., & Baylor, S. M. (2012). Measurement and simulation of myoplasmic calcium transients in mouse slow-twitch muscle fibres. *The Journal of Physiology*, *590*(3), 575–594. https://doi.org/10.1113/jphysiol.2011.220780

Hollý, M., & Poledna, J. (1989). Model of calcium diffusion, binding and membrane transport in the sarcomere of frog skeletal muscle. *General Physiology and Biophysics*, *8*(6), 539–553. http://www.ncbi.nlm.nih.gov/pubmed/2533126

Hudecova, S., Vadaszova, A., Soukup, T., & Krizanova, O. (2004). Effect of thyroid hormones on the gene expression of calcium transport systems in rat muscles. *Life Sciences*, *75*(8), 923–931. https://doi.org/10.1016/j.lfs.2004.01.026

Jackman, M. R., & Willis, W. T. (1996). Characteristics of mitochondria isolated from type I and type IIb skeletal muscle. *American Journal of Physiology-Cell Physiology*, *270*(2), C673–C678. https://doi.org/10.1152/ajpcell.1996.270.2.C673

James, & Keener. (2009). *Mathematical Physiology: Vol. 8/1* (J. Keener & J. Sneyd (eds.)). Springer New York. https://doi.org/10.1007/978-0-387-75847-3

Jorgensen, A. O., Kalnins, V., & MacLennan, D. H. (1979). Localization of sarcoplasmic reticulum proteins in rat skeletal muscle by immunofluorescence. *Journal of Cell Biology*, *80*(2), 372–384. https://doi.org/10.1083/jcb.80.2.372

Konishi, M., Suda, N., & Kurihara, S. (1993). Fluorescence signals from the Mg2+/Ca2+ indicator furaptra in frog skeletal muscle fibers. *Biophysical Journal*, *64*(1), 223–239. https://doi.org/10.1016/S0006-3495(93)81359-6

Kushmerick, M. J., Moerland, T. S., & Wiseman, R. W. (1992). Mammalian skeletal muscle fibers distinguished by contents of phosphocreatine, ATP, and Pi. *Proceedings of the National Academy of Sciences of the United States of America*, *89*(16), 7521–7525. https://doi.org/10.1073/PNAS.89.16.7521

Lamb, G. D., & Walsh, T. (1987). Calcium currents, charge movement and dihydropyridine binding in fast- and slow-twitch muscles of rat and rabbit. *The Journal of Physiology*, *393*(1), 595–617. https://doi.org/10.1113/jphysiol.1987.sp016843

Leberer, E., & Pette, D. (1986). Immunochemical quantification of sarcoplasmic reticulum Ca-ATPase, of calsequestrin and of parvalbumin in rabbit skeletal muscles of defined fiber composition. *European Journal of Biochemistry*, *156*(3), 489–496. http://www.ncbi.nlm.nih.gov/pubmed/2938950

Lee, Y. S., Ondrias, K., Duhl, A. J., Ehrlich, B. E., & Kim, D. H. (1991). Comparison of calcium release from sarcoplasmic reticulum of slow and fast twitch muscles. *The Journal of Membrane Biology*, *122*(2), 155–163. https://doi.org/10.1007/BF01872638

Linck, B., Qiu, Z., He, Z., Tong, Q., Hilgemann, D. W., & Philipson, K. D. (1998). Functional comparison of the three isoforms of the Na+/Ca2+ exchanger (NCX1, NCX2, NCX3). *American Journal of Physiology - Cell Physiology*, *274*(2 43-2). https://doi.org/10.1152/ajpcell.1998.274.2.c415

Liu, W., & Olson, S. D. (2015). Compartment calcium model of frog skeletal muscle during activation. *Journal of Theoretical Biology*, *364*, 139–153. https://doi.org/10.1016/j.jtbi.2014.08.050

Lytton, J., Westlin, M., Burk, S. E., Shull, G. E., & MacLennan, D. H. (1992). Functional comparisons between isoforms of the sarcoplasmic or endoplasmic reticulum family of calcium pumps. *The Journal of Biological Chemistry*, *267*(20), 14483–14489. http://www.ncbi.nlm.nih.gov/pubmed/1385815

Marcucci, L., Canato, M., Protasi, F., Stienen, G. J. M., & Reggiani, C. (2018). A 3D diffusional-compartmental model of the calcium dynamics in cytosol, sarcoplasmic reticulum and mitochondria of murine skeletal muscle fibers. *PLOS ONE*, *13*(7), e0201050. https://doi.org/10.1371/journal.pone.0201050

Milán, Rincon, Giraldo, & Calderon. (2021). Calibration of mammalian skeletal muscle Ca2+ transients recorded with the fast Ca2+ dye Mag-Fluo-4. *Submitted*.

Murphy, R. M., Larkins, N. T., Mollica, J. P., Beard, N. A., & Lamb, G. D. (2009). Calsequestrin content and SERCA determine normal and maximal Ca^{2+} storage levels in sarcoplasmic reticulum of fast- and slow-twitch fibres of rat. *The Journal of Physiology*, *587*(2), 443–460.

https://doi.org/10.1113/jphysiol.2008.163162

Needham, D. M. (1926). Red and white muscle. *Physiological Reviews*, *6*(1), 1–27. https://doi.org/10.1152/physrev.1926.6.1.1

Periasamy, M., & Kalyanasundaram, A. (2007). SERCA pump isoforms: Their role in calcium transport and disease. *Muscle & Nerve*, *35*(4), 430–442. https://doi.org/10.1002/mus.20745

Potter, J. D., & Gergely, J. (1975). The calcium and magnesium binding sites on troponin and their role in the regulation of myofibrillar adenosine triphosphatase. *The Journal of Biological Chemistry*, *250*(12), 4628–4633. http://www.ncbi.nlm.nih.gov/pubmed/124731

Racay, P., Gregory, P., & Schwaller, B. (2006). Parvalbumin deficiency in fast-twitch muscles leads to increased "slow-twitch type" mitochondria, but does not affect the expression of fiber specific proteins. *FEBS Journal*, *273*(1), 96–108. https://doi.org/10.1111/j.1742-4658.2005.05046.x

Ranvier, & M L. (1873). Properties et structures differentes des muscles blancs, chez les lapins et chez le raies. *CR Hedd Acad Sci*, *77*, 1030.

Renganathan, M., Messi, M. L., & Delbono, O. (1998). Overexpression of IGF-1 exclusively in skeletal muscle prevents age- related decline in the number of dihydropyridine receptors. *Journal of Biological Chemistry*, *273*(44), 28845–28851. https://doi.org/10.1074/jbc.273.44.28845

Ridgway, E. B., & Ashley, C. C. (1967). Calcium transients in single muscle fibers. *Biochemical and Biophysical Research Communications*, *29*(2), 229–234. http://www.ncbi.nlm.nih.gov/pubmed/4383681

Robertson, S. P., Johnson, J. D., & Potter, J. D. (1981). The time-course of Ca2+ exchange with calmodulin, troponin, parvalbumin, and myosin in response to transient increases in Ca2+. *Biophysical Journal*, *34*(3), 559. https://doi.org/10.1016/S0006-3495(81)84868-0

Rolfe, D. F. S., & Brown, G. C. (1997). Cellular energy utilization and molecular origin of standard metabolic rate in mammals. *Physiological Reviews*, *77*(3), 731–758. https://doi.org/10.1152/physrev.1997.77.3.731

Sacchetto, R., Margreth, A., Pelosi, M., & Carafoli, E. (1996). Colocalization of the dihydropyridine receptor, the plasma-membrane calcium ATPase isoform 1 and the sodium/calcium exchanger to the junctional-membrane domain of transverse tubules of rabbit skeletal muscle. *European Journal of Biochemistry*, *237*(2), 483–488.

http://www.ncbi.nlm.nih.gov/pubmed/8647089

Schiaffino, S., Gorza, L., Sartore, S., Saggin, L., Ausoni, S., Vianello, M., Gundersen, K., & LØmo, T. (1989). Three myosin heavy chain isoforms in type 2 skeletal muscle fibres. *Journal of Muscle Research and Cell Motility*, *10*(3), 197–205. https://doi.org/10.1007/BF01739810

Schiaffino, S., & Reggiani, C. (2011). Fiber Types in Mammalian Skeletal Muscles. *Physiological Reviews*, *91*(4), 1447–1531. https://doi.org/10.1152/physrev.00031.2010

Schwerzmann, K., Hoppeler, H., Kayar, S. R., & Weibel, E. R. (1989). Oxidative capacity of muscle and mitochondria: correlation of physiological, biochemical, and morphometric characteristics. *Proceedings of the National Academy of Sciences of the United States of America*, *86*(5), 1583–1587. http://www.ncbi.nlm.nih.gov/pubmed/2922400

Sembrowich, W. L., Quintinskie, J. J., & Li, G. (1985). Calcium uptake in mitochondria from different skeletal muscle types. *Journal of Applied Physiology*, *59*(1), 137–141. https://doi.org/10.1152/jappl.1985.59.1.137

Sperelakis, N. (2012). Cell Physiology Source Book. In *Cell Physiology Source Book*. Elsevier Inc. https://doi.org/10.1016/C2010-0-66479-0

Wang, J. H. (1953). Tracer-diffusion in Liquids. IV. Self-diffusion of Calcium Ion and Chloride Ion in Aqueous Calcium Chloride Solutions 1. *Journal of the American Chemical Society*, *75*(7), 1769–1770. https://doi.org/10.1021/ja01103a539

Wang, M., Sun, J., & Yang, Q. (2020). Modeling and simulation of excitation- contraction coupling of fast-twitch skeletal muscle fibers. *Technology and Health Care*, *28*, 13–24. https://doi.org/10.3233/THC-209003

Westerblad, H., & Allen, D. G. (1992). Myoplasmic free Mg2+ concentration during repetitive stimulation of single fibres from mouse skeletal muscle. *The Journal of Physiology*, *453*, 413–434. http://www.ncbi.nlm.nih.gov/pubmed/1464836

Westerblad, H., & Allen, D. G. (1994). The role of sarcoplasmic reticulum in relaxation of mouse muscle; effects of 2,5-di(tert-butyl)-1,4-benzohydroquinone. *The Journal of Physiology*, *474*(2), 291–301. http://www.ncbi.nlm.nih.gov/pubmed/8006816

Williams, D. A., Head, S. I., Bakker, A. J., & Stephenson, D. G. (1990).

Resting calcium concentrations in isolated skeletal muscle fibres of dystrophic mice. *The Journal of Physiology*, *428*, 243–256. http://www.ncbi.nlm.nih.gov/pubmed/2231412

Wüst, R. C. I., Helmes, M., Martin, J. L., van der Wardt, T. J. T., Musters, R. J. P., van der Velden, J., & Stienen, G. J. M. (2017). Rapid frequency-dependent changes in free mitochondrial calcium concentration in rat cardiac myocytes. *The Journal of Physiology*, *595*(6), 2001–2019. https://doi.org/10.1113/JP273589

Publications and works in scientific meetings

Article in Biochimica et Biophysica Acta (BBA)-General Subjects. 2021. Calibration of mammalian skeletal muscle Ca^{2+} transients recorded with the fast Ca^{2+} dye Mag-Fluo-4. https://doi.org/10.1016/j.bbagen.2021.129939.

Article submitted to Journal of General Physiology (2021). Comprehensive simulation of Ca^{2+} transients in the continuum of mouse skeletal muscle fiber types.

Poster in Biophysical Society 64th Annual Meeting. 2020. Simulation of Ca^{2+} movements during single Ca^{2+} transients in the continuum of mammalian skeletal muscle fiber types, including Na^{+}/Ca^{2+} exchanger and mitochondria.

Video poster in Sociedad Chilena de Ciencias Fisiológicas (SCHCF) + Asociación Latinoamericana de Ciencias Fisiológicas (ALACF) joint meeting. 2020. Experimental and mathematical study of the excitation-contraction coupling in murine skeletal muscle fibers using the fast Ca^{2+} dye Mag-Fluo-4. The abstract of the video poster is available in the following link (pages 82 and 83): https://pmr.safisiol.org.ar/archive/id/122.